

---

# Why Tree-Style Branching Matters for Thought Advantage Estimation in GRPO

---

Hongcheng Wang<sup>\*1,2</sup> Yinuo Huang<sup>\*3,2</sup> Sukai Wang<sup>4</sup> Guanghui Ren<sup>+4</sup> Hao Dong<sup>1,2</sup>

## Abstract

Group Relative Policy Optimization (GRPO) trains Chain-of-Thought reasoning with verifiable rewards, but estimating thought-level advantages without value functions often suffers from high variance. Although tree-style branching is used in practice to reduce the variance, it lacks a theoretical explanation of why it works and whether it is important or even potentially necessary. We study thought-level advantage estimation in GRPO from a variance perspective under a minimal tree-style setting where multiple answers are sampled for each thought. Using the multivariate delta method, we reveal an asymmetry in how different sampling dimensions affect variance. Increasing the number of sampled thoughts ( $K$ ) leaves a strictly positive variance floor, whereas increasing the number of answers per thought ( $M$ ) induces a monotonic decrease in variance, asymptotically decreasing it to zero. This implies that accurate thought-level advantage estimation is impossible through scaling thought sampling alone, making branching a potentially necessary mechanism rather than a heuristic. Experiments further provide empirical evidence for both the effectiveness and necessity of answer-level branching, demonstrating improved optimization stability, training efficiency, and final performance not only in math but also across a broad range of vision domains and under different model architectures and sizes.

## 1. Introduction

The DeepSeek-R1 model demonstrates that reinforcement learning (RL)—particularly Group Relative Policy Optimization (GRPO) (Shao et al., 2024)—is effective for training Chain-of-Thought (CoT) reasoning. GRPO prompts the LLM to generate a reasoning trace before producing

<sup>\*</sup>Equal contribution <sup>+</sup>Project Lead <sup>1</sup>CFCS, School of Computer Science, Peking University, Beijing, China <sup>2</sup>PKU–Agibot Joint Lab, Beijing, China <sup>3</sup>University of Electronic Science and Technology of China, Chengdu, China <sup>4</sup>Agibot, Beijing, China. Correspondence to: Hao Dong <hao.dong@pku.edu.cn>.

the final answer and then reinforces this process via verifiable rewards. Subsequent methods such as DAPO (Yu et al., 2025), Dr.GRPO (Liu et al., 2025), and GPG (Chu et al., 2025) refine GRPO’s loss function from different perspectives, achieving more stable training and stronger mathematical reasoning. Beyond text-based tasks, the GRPO paradigm has also expanded to multi-modal domains (Chen et al., 2025; Shen et al., 2025; Huang et al., 2025b; Feng et al., 2025; Song et al., 2025; Kim et al., 2025), where task-specific reward designs are adopted to improve performance under diverse objectives. Collectively, these results demonstrate that CoT combined with verifiable RL rewards substantially enhances reasoning across modalities.

Although GRPO has demonstrated strong empirical performance across a wide range of domains, it still suffers from instability in thought-level advantage estimation. In standard GRPO-style algorithms, each thought is typically evaluated using a single sampled answer, which contributes to high-variance advantage estimates and unstable gradient updates during training. A growing body of recent work (Kazemnejad et al., 2024; Li et al., 2025; Yang et al., 2025; Guo et al., 2025) empirically adopts tree-style branching to improve the stability of GRPO-style training. However, most of these tree-style methods primarily demonstrate effectiveness through empirical results only on mathematical tasks, rely on complex heuristic segmentation or branching rules, and lack a principled theoretical explanation of *why* branching improves learning. More importantly, they do not address whether such branching is merely a helpful heuristic or necessary for accurate thought advantage estimation when using GRPO-style, group-normalized advantage estimators without value models.

In this work, we build upon the empirical successes of *tree-style branching* in GRPO-style training and take a complementary theoretical perspective, focusing on the variance properties of thought-level advantage estimation. To facilitate principled analysis, we simplify the branching mechanism and consider a minimal form of tree search: instead of introducing complex segment- or step-level branching rules, we perform branching only at the answer level. Concretely, we delimit each thought using an explicit XML tag (e.g., `</think>`) and sample multiple answers conditioned on the same thought. We name this mechanism **GRPO-MA (GRPO with Multi-Answer)**.

Under this formulation, we analyze thought-level advantage estimation in GRPO from a variance perspective and derive an approximate variance characterization using the multivariate delta method. Our analysis goes beyond the observation that increasing the total number of samples reduces variance, and instead **reveals a fundamental asymmetry between different sampling dimensions**. Concretely, under GRPO-style group-normalized estimators without value models, increasing the number of independently sampled thoughts ( $K$ ) alone cannot eliminate thought advantage estimation noise: the variance converges to **a strictly positive constant**, regardless of how large  $K$  becomes. In contrast, increasing the number of answers per thought ( $M$ ) suppresses the estimation noise along a different sampling dimension, **monotonically decreasing the thought-level advantage variance to zero**. Together, these results clarify the distinct statistical roles of the two sampling dimensions and explain why tree-style branching is consistently effective in practice. More importantly, they establish that such branching is not merely a heuristic, but a principled and *potentially necessary* mechanism for accurate thought-level advantage estimation *under GRPO-style estimators without value models*.

Beyond theory, our experiments using GRPO-MA provide direct empirical evidence for both the *effectiveness* and the *necessity* of answer-level branching in GRPO-style training. Comparing T4A1<sup>1</sup> and T4A4, we show that answer-level branching consistently improves performance across diverse domains. More importantly, comparing T4A4 with a thought-scaling baseline T16A1 reveals a *strictly better efficiency–performance trade-off*: despite operating at substantially lower computational cost, T4A4 achieves slightly better final performance. This indicates that answer-level branching is not merely an efficiency optimization, but a *necessary design choice* under GRPO-style training, as it enables simultaneous gains in both efficiency and performance. Moreover, T4A4 exhibits significantly fewer gradient spikes than T16A1, as measured by the Gradient Spike Score (GSS), consistent with our variance analysis that lower-variance advantage estimation leads to more stable optimization. Across multiple tasks, model sizes, and architectures, these benefits are robust and not task- or model-specific. Our contributions are summarized as follows:

- **Asymmetric variance in advantage estimation.** We present the first variance-based analysis of thought-level advantage estimation in GRPO-style algorithms using the multivariate delta method. Our analysis reveals a fundamental asymmetry in how different sam-

pling dimensions affect the variance of the estimated advantages, explaining why branching is effective and potentially necessary for reliable advantage estimation under GRPO-style estimators.

- **GRPO-MA: a minimal tree-style instantiation.** Motivated by this analysis, we propose GRPO-MA, a lightweight and stable instantiation of tree-style branching that introduces answer-level branching via explicit semantic delimiters natively supported by GRPO, requiring minimal modifications and virtually no additional hyperparameters.
- **Broad empirical effectiveness across tasks and model configurations.** Extensive experiments across mathematics, code generation, vision, and embodied manipulation, as well as models of different sizes and architectures, demonstrate that GRPO-MA consistently outperforms standard GRPO and achieves a strictly better efficiency–performance trade-off than thought-scaling GRPO baselines..

## 2. Related Work

### 2.1. GRPO Stabilization via Objective and Gradients

A line of work improves the stability and efficiency of GRPO-style training by revisiting the objective, advantage computation, and gradient estimation. DAPO (Yu et al., 2025) combines several practical techniques, including exploration-aware clipping (Clip-Higher), dynamic filtering of uninformative samples (Dynamic Sampling), and a token-level policy-gradient loss to better weight long reasoning traces. Dr. GRPO (Liu et al., 2025) mitigates response-length and question-difficulty biases by removing specific normalization terms in the loss and advantage calculations. GPG (Chu et al., 2025) simplifies the GRPO objective and introduces gradient rescaling to reduce the impact of “zero-gradient” samples. Related methods further target stability from complementary angles: GSPO (Zheng et al., 2025) realigns importance sampling at the sequence level, GMPO (Zhao et al., 2025) uses geometric-mean aggregation to reduce sensitivity to outliers, and GTPO (Simoni et al., 2025) analyzes trajectories to resolve gradient conflicts and prevent policy collapse.

### 2.2. Tree Search in LLMs Reinforcement Learning

Recent research has shifted from independent chain-based rollouts to tree-structured sampling to enhance exploration efficiency and credit assignment. VinePPO (Kazemnejad et al., 2024) performing Monte Carlo value estimation through multiple suffix rollouts. Evolving from this, SPO (Guo et al., 2025) generalizes the concept of segmentation, enabling flexible granularity advantage estimation. TreeRL (Hou et al., 2025) introduced an entropy-guided

<sup>1</sup>TKAM denotes a GRPO-style sampling configuration with  $K$  thoughts and  $M$  answers per thought;  $M=1$  corresponds to standard GRPO, while  $M>1$  corresponds to GRPO-MA. The same notation is used in the experiments.

search strategy that expands the search at high-uncertainty tokens. TreePO (Li et al., 2025) estimating advantages based on the collective outcomes of grouping sub-trees, improving robustness. TreeRPO (Yang et al., 2025) defines tree nodes at the level of reasoning steps and derive step-wise supervision by propagating outcome rewards across sibling branches.

A key distinction among prior tree-search methods lies in where branching is introduced along the generation process. In this work, we adopt semantic XML tags (e.g., `</think>`) as branching points, which provide a simple and implementation-friendly instantiation. However, the primary goal of this paper is not to advocate a particular branching heuristic as optimal. Instead, we intentionally focus on a simplified and concrete branching scheme to facilitate a principled analysis of why branching is effective, and more importantly, why it is potentially necessary under the GRPO-style advantage estimator.

### 3. Preliminary: GRPO

GRPO (Shao et al., 2024) is a PPO-style algorithm (Schulman et al., 2017) that computes advantages by normalizing rewards from  $K$  sampled responses. For a prompt  $p$ , GRPO generates responses  $\{o_i\}_{i=1}^K$  with rewards  $\{R_i\}$  and computes  $A(o_i) = \frac{R_i - \text{Mean}(\{R_k\})}{\text{Std}(\{R_k\})}$ . The complete GRPO objective can be written as:

$$\begin{aligned} \mathcal{J}_{\text{GRPO}}(\theta) &= \mathbb{E}_{\substack{(p,a) \sim \mathcal{D} \\ o \sim \pi_{\theta_{\text{old}}}}} \left[ \frac{1}{K} \sum_{i=1}^K \frac{1}{T_i^o} \sum_{t=1}^{T_i^o} \ell_{\text{clip}}(r_t, A(o_i)) \right] \\ &\quad - \beta D_{\text{KL}}(\pi_{\theta} \parallel \pi_{\text{ref}}). \end{aligned} \quad (1)$$

where  $T_i^o$  denotes the length of the  $i$ -th output trajectory  $o_i = (o_{i,1}, \dots, o_{i,T_i^o})$ . The term  $r_t$  is the per-token likelihood ratio,  $r_t = \frac{\pi_{\theta}(o_{i,t}|p, o_{i,<t})}{\pi_{\theta_{\text{old}}}(o_{i,t}|p, o_{i,<t})}$ , where  $\pi_{\theta}$  and  $\pi_{\theta_{\text{old}}}$  denote the current and behavior policies used for on-policy sampling. We use the shorthand  $\ell_{\text{clip}}(r, A) \triangleq \min(rA, \text{clip}(r, 1 \pm \varepsilon)A)$  for the clipped surrogate term.

As indicated by Equation 1, the advantage determines whether the probability of a certain token increases or decreases, as well as the magnitude of this change. Therefore, a more stable estimation of the advantage (with lower variance) is beneficial for a more stable model parameter update.

## 4. Method

In this section, we first describe the sampling and updating process of GRPO-MA, which builds upon the GRPO framework by introducing a multi-answer sampling strategy. We then analyze the variance change of the advantages via the

delta method.

### 4.1. Pipeline of GRPO-MA

The core modification in GRPO-MA lies in its sampling pipeline, shown in Fig. 1. Given a prompt  $p$ , it first generates  $K$  thoughts  $\{th_1, \dots, th_K\}$  identically to GRPO. Then, for each thought  $th_i$ , GRPO-MA then generates  $M$  answers  $\{ans_{i,1}, \dots, ans_{i,M}\}$ , resulting in  $K \times M$  total answers where every  $M$  answers share the same thought.

After obtaining rewards  $\{R_{i,j}\}_{1 \leq i \leq K, 1 \leq j \leq M}$  from a reward function, we define the value of a thought as  $V(th_i) = \frac{1}{M} \sum_{j=1}^M R_{i,j}$ , and normalize it to compute the thought advantage  $A(th_i) = \frac{V(th_i) - \text{Mean}(\{V(th_k)\}_{1 \leq k \leq K})}{\text{Std}(\{V(th_k)\}_{1 \leq k \leq K})}$ . Similarly, the advantage of an answer is  $A(ans_{i,j}) = \frac{R_{i,j} - \text{Mean}(\{R_{k,l}\}_{1 \leq k \leq K, 1 \leq l \leq M})}{\text{Std}(\{R_{k,l}\}_{1 \leq k \leq K, 1 \leq l \leq M})}$ .

The GRPO-MA objective then combines the two levels of advantages:

$$\begin{aligned} \mathcal{J}_{\text{GRPO-MA}}(\theta) &= \mathbb{E}_{\substack{(p,a) \sim \mathcal{D} \\ th \sim \pi_{\theta_{\text{old}}}}} \left[ \frac{1}{K} \sum_i \frac{1}{T_i^{\text{th}}} \sum_{t=1}^{T_i^{\text{th}}} \ell_{\text{clip}}(r_t, A(th_i)) \right] \\ &\quad + \mathbb{E}_{\text{ans} \sim \pi_{\theta_{\text{old}}}} \left[ \frac{1}{KM} \sum_{i,j} \frac{1}{T_{i,j}^{\text{ans}}} \sum_{t=1}^{T_{i,j}^{\text{ans}}} \ell_{\text{clip}}(r_t, A(ans_{i,j})) \right] \\ &\quad - \beta D_{\text{KL}}(\pi_{\theta} \parallel \pi_{\text{ref}}). \end{aligned} \quad (2)$$

where  $T_i^{\text{th}}$  and  $T_{i,j}^{\text{ans}}$  denote the lengths of the thought trajectory  $th_i$  and the answer trajectory  $ans_{i,j}$ , respectively. The term  $A(th_i)$  is the thought-level advantage computed by aggregating the rewards of the  $M$  answers associated with  $th_i$ , while  $A(ans_{i,j})$  denotes the advantage of an individual answer. The remaining notation follows the same definitions as in the GRPO objective.

### 4.2. Variance of the Thought Advantage

#### 4.2.1. PRELIMINARIES

Fix a prompt  $p$ . We sample  $K$  thoughts  $th_i \stackrel{\text{i.i.d.}}{\sim} \pi_{\theta}(\cdot | p)$ , and for each  $th_i$  sample  $M$  answers  $ans_{i,j} \sim \pi_{\theta}(\cdot | p, th_i)$ . Each answer is scored by a deterministic reward function, defining  $R_{i,j} := r(p, ans_{i,j})$ .

Let  $\mu_{R_i} := \mathbb{E}[R_{i,j} | p, th_i]$  and  $\sigma_{R_i}^2 := \text{Var}(R_{i,j} | p, th_i)$ , where  $\{R_{i,j}\}_{j=1}^M$  are i.i.d. conditional on  $(p, th_i)$ .

The empirical thought value  $V(th_i) := \frac{1}{M} \sum_{j=1}^M R_{i,j}$  then satisfies  $\mathbb{E}[V(th_i) | p, th_i] = \mu_{R_i}$  and  $\text{Var}(V(th_i) | p, th_i) = \sigma_{R_i}^2 / M$ .

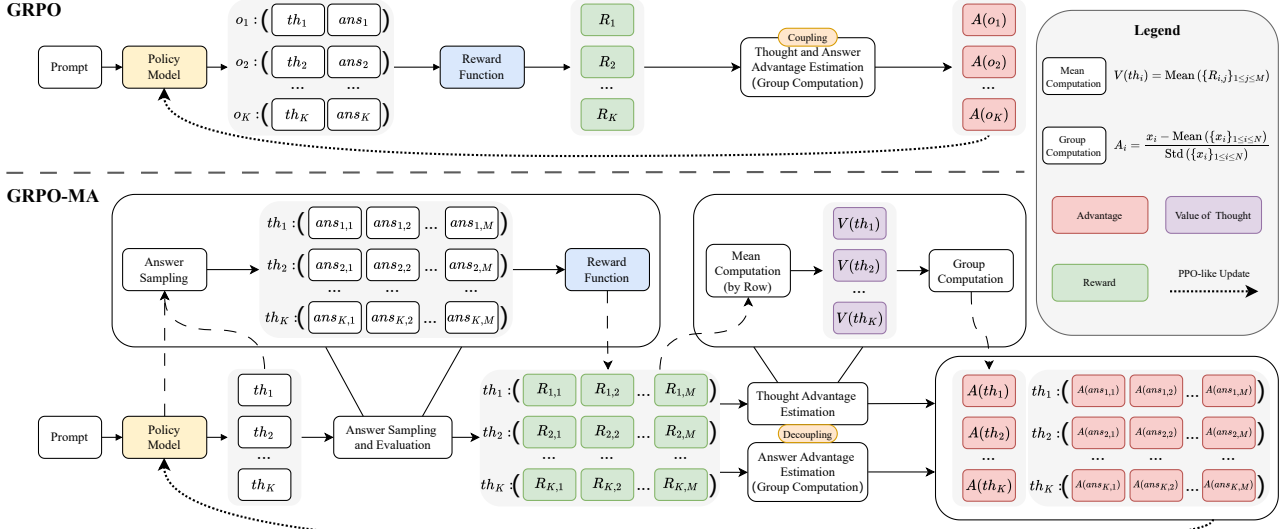


Figure 1. The operational flow of advantage estimation in GRPO and GRPO-MA. In the baseline GRPO framework (top), the advantage is computed from a single thought–answer pair, inherently coupling the estimation of thought and answer advantages to a single reward signal. In contrast, GRPO-MA (bottom) extends this setting by sampling multiple answers for each thought.

**Independence assumption.** We assume  $\{V(th_i)\}_{i=1}^K$  are mutually independent, *i.e.*, the covariance matrix is diagonal. While mild correlations may arise from sharing the same prompt, Appendix C.5 shows that diagonal terms dominate the covariance structure, making this assumption reasonable.

#### 4.2.2. APPROXIMATE VARIANCE ESTIMATION

Using the first-order multivariate delta method, and noting that under the independence assumption the covariance matrix of  $\{V(th_k)\}$  is diagonal, the variance of the standardized thought advantage is approximated as

$$\text{Var}[A(th_i)] \approx \frac{1}{M \sigma_{\mu_R}^2} \sum_{k=1}^K \left( \delta_{ik} - \frac{1}{K} - \frac{\tilde{\mu}_i \tilde{\mu}_k}{K-1} \right)^2 \sigma_{R_k}^2 \quad (3)$$

where  $\delta_{ik}$  is the Kronecker delta ( $\delta_{ik} = 1$  if  $i = k$ , and 0 otherwise),  $\mu_{\bar{R}} = \frac{1}{K} \sum_{k=1}^K \mu_{R_k}$  is the average true thought value,  $\sigma_{\mu_R}^2 = \frac{1}{K-1} \sum_{k=1}^K (\mu_{R_k} - \mu_{\bar{R}})^2$  is the variance of the true thought values across thoughts,  $\tilde{\mu}_i = \frac{\mu_{R_i} - \mu_{\bar{R}}}{\sigma_{\mu_R}}$  is the normalized (expected) advantage of thought  $th_i$ .

**For the full derivation on the variance of though advantages and answer advantages, please refer to Appendix C.**

#### 4.2.3. CONTROLLABLE AND UNCONTROLLABLE SOURCES OF VARIANCE.

Apart from the sampling dimensions  $K$  and  $M$ , the remaining terms in Eq. (3) depend on the particular sampled

thoughts and vary stochastically across iterations. Within the GRPO-style estimator considered here, these quantities are not directly controllable by the learning algorithm. To the best of our knowledge, there is currently no stable and generally applicable method to control them in GRPO-style training. Even if such methods were to exist, they would be complementary to answer-level branching rather than a substitute. Accordingly,  $K$  and  $M$  constitute the primary controllable parameters for variance control in our analysis.

#### 4.2.4. ANALYSIS OF THE VARIANCE STRUCTURE

Combining the above results, we now compare the effects of increasing the number of sampled thoughts  $K$  versus increasing the number of answers  $M$  for each thought.

As  $K \rightarrow \infty$ , by the law of large numbers, the sample variance of the true thought values,

$$\sigma_{\mu_R}^2 = \frac{1}{K-1} \sum_{k=1}^K (\mu_{R_k} - \mu_{\bar{R}})^2,$$

converges almost surely to the population variance

$$\sigma_{\pi}^2 = \text{Var}_{th \sim \pi_{\theta}(\cdot|p)}[E[V(th) | p, th]].$$

which characterizes the intrinsic variability of true thought values across the population induced by the policy  $\pi_{\theta}$  and prompt  $p$ .

To analyze the remaining terms in the variance expression, we decompose the relevant summation according to the Kronecker delta  $\delta_{ik}$ . The single term with  $k = i$  converges to a non-zero constant, since expressions of the form  $(\delta_{ik} -$

$\frac{1}{K} - \dots$ ) approach 1 as  $K \rightarrow \infty$ . In contrast, each of the remaining  $K - 1$  terms with  $k \neq i$  is of order  $O(1/K^2)$ , and therefore their total contribution vanishes at rate  $O(1/K)$ .

As a result, for any fixed number of answers  $M < \infty$ , the variance of the advantage estimator converges to a strictly positive limit:

$$\lim_{K \rightarrow \infty} \text{Var}[A(th_i)] = \frac{\sigma_{R_i}^2}{M \sigma_{\pi}^2}.$$

This limit depends only on the intrinsic response variance  $\sigma_{R_i}^2$  of the thought  $th_i$  and the population-level variance  $\sigma_{\pi}^2$ , and cannot be further reduced by increasing  $K$  alone when  $M$  is held fixed.

In contrast, for any fixed number of sampled thoughts  $K < \infty$ , increasing the number of answers  $M$  directly suppresses the variance of the estimated thought advantage. In this regime, the variance scales inversely with  $M$ , and thus

$$\lim_{M \rightarrow \infty} \text{Var}[A(th_i)] = 0, \text{ with } \text{Var}[A(th_i)] = O\left(\frac{1}{M}\right).$$

These results reveal a fundamental asymmetry in thought-level advantage estimation under GRPO-style training without value models. Increasing the number of sampled thoughts  $K$  yields no predictable variance reduction at finite  $K$  and is only guaranteed to converge to a strictly positive variance floor as  $K \rightarrow \infty$ . In contrast, increasing the number of answers per thought  $M$  induces a monotonic and controllable reduction in variance, decreasing it to zero as  $M$  increases. As a result, effective variance reduction cannot be achieved through thought expansion alone. Absent additional mechanisms for directly controlling thought content, tree-style branching that induces multiple answers per thought becomes potentially necessary for stabilizing thought advantage estimation.

## 5. Experiments

We evaluate GRPO-MA on Math (Yu et al., 2025), Code (PrimeIntellect, 2024; White et al., 2024), several distinct vision tasks (Object Detection (contributors, 2024), Affordance Prediction (Myers et al., 2015; Luo et al., 2022), Trajectory Prediction (Ji et al., 2025), Demand Prediction (Wang et al., 2024), OCR-based VQA (Biten et al., 2019; Tito et al., 2021)) and a Simulator-based Visual Manipulation task (Li et al., 2024). Our experiments use Qwen2.5-VL-3B-Instruct (Bai et al., 2025) as the base model, with all training conducted on four H100 80G GPUs using LoRA (Hu et al., 2022) for parameter-efficient fine-tuning. For each task, we conduct a group of experiments separately.

**More details (tasks, datasets, hyperparameters, training settings) are in the appendix D and E.**

Table 1. Evaluation metrics for each task.

Task	Evaluation Metric
<b>Math</b>	Pass@k (Chen et al., 2021b)
<b>Code</b>	Pass@k
<b>Object Detection</b>	Accuracy: proportion of predictions with IoU > threshold.
<b>Affordance Prediction</b>	Accuracy: proportion of correctly matched points.
<b>Trajectory Prediction</b>	DFD (Eiter et al., 1994), HD (Huttenlocher et al., 2002), RMSE, EndPoint Dist.
<b>Demand Prediction</b>	Accuracy: proportion of correct points.
<b>OCR-based VQA</b>	ANLS (Biten et al., 2019)

### 5.1. Text and Vision Task

#### 5.1.1. TASK SETTING AND METRIC

Table 1 summarizes evaluation metrics for text and vision tasks. These tasks collectively cover a wide range of modalities and reasoning types, enabling a comprehensive evaluation of GRPO-MA.

For **Math**, we adopt a structured output format using `<analysis>`, `<process>`, and `<answer>` tags. GRPO-MA applies multi-sampling on both `<process>` and `<answer>`. For all other tasks, multi-sampling is applied only to `<answer>`.

We track the **Gradient Spike Score (GSS)** (Huang et al., 2025a) to measure gradient stability, defined as  $GSS(g_i) = \frac{|g_i|}{\frac{1}{T+1} \sum_{j=0}^T |g_j|}$ , where  $g_j$  represents the gradient at the  $j$ -th time step. We report the number of spikes above 10 (GSS@10), where smaller is better.

#### 5.1.2. BASELINES

We adopt models from the Qwen2.5-VL-Instruct series (3B, 7B, and 72B) (Bai et al., 2025) as baselines to evaluate the performance of general-purpose models on our tasks. In addition, we train Qwen2.5-VL-3B-Instruct with real labels using supervised fine-tuning (SFT) to compare against GRPO, denoted as **SFT** in the results. Finally, we compare our proposed GRPO-MA with GRPO under different numbers of responses to demonstrate the superiority of GRPO-MA in terms of training efficiency and performance.

#### 5.1.3. MAIN RESULTS ON TEXT AND VISION TASK

The experimental results are presented in Tab. 2 (Math and Code), Tab. 3 (Object Detection, Affordance Prediction, and Demand Prediction), and Tab. 4 (OCR-based VQA and Trajectory Prediction). Across multiple tasks, our proposed GRPO-MA consistently outperforms both GRPO and

## Why Tree-Style Branching Matters

Table 2. Combined Results for Math and Code Generation Benchmarks. TN: The number of thoughts; AN: The number of answers per thought; S/S: Second/Step during training; Bold indicates the best performance among the GRPO variants.

Model	TN AN		Math				Code			
			S/S	GSS	Pass@10(N=100)	Pass@32(N=100)	S/S	GSS	Pass@10(N=100)	Pass@32(N=100)
Qwen2.5-VL-3B-Ins					9.27	16.25			9.80	11.67
Qwen2.5-VL-7B-Ins					9.97	18.39			10.72	11.31
Qwen2.5-VL-72B-Ins					33.07	41.39			20.39	22.37
SFT					11.07	18.11			8.72	10.59
GRPO	4	1	111.24	<b>5</b>	11.78	20.32	76.21	<b>6</b>	11.56	13.70
GRPO	8	1	140.05	13	11.16	21.30	104.83	24	11.44	13.39
GRPO	16	1	225.43	15	12.89	21.72	186.91	25	<b>11.92</b>	14.12
GRPO-MA	4	4	132.87	<b>5</b>	<b>14.70</b>	<b>27.60</b>	93.45	10	11.69	<b>14.70</b>

Table 3. Combined Results for Object Detection, Affordance, and Demand Prediction. TN: The number of thoughts; AN: The number of answers per thought; S/S: Second/Step during training; UMD: UMD Part Affordance Dataset; AGD20K: AGD20K Dataset; Bold indicates the best performance among models of the same size.

Model	TN AN		Object Detection				Affordance Prediction				Demand Prediction				
			S/S	GSS@10	IoU@0.5	IoU@0.6	IoU@0.7	IoU@0.8	S/S	GSS@10	UMD	AGD20K	S/S	GSS	Accuracy
Qwen2.5-VL-3B					60.87	50.54	39.67	21.32			38.98	52.73			11.41
Qwen2.5-VL-7B					70.11	60.23	48.02	25.89			34.65	43.29			19.95
Qwen2.5-VL-72B					72.57	60.66	47.19	24.48			59.13	60.59			26.27
SFT					64.63	54.73	42.43	22.96			66.35	53.18			36.97
GRPO	4	1	13.86	5	65.11	56.16	43.88	23.02	14.34	11	78.91	55.60	13.74	<b>5</b>	38.13
GRPO	8	1	18.86	30	67.13	57.52	42.62	22.82	18.92	14	88.14	57.90	18.20	12	40.81
GRPO	16	1	26.99	16	69.03	60.29	45.16	24.04	24.27	22	89.32	57.24	25.42	37	42.47
GRPO-MA	4	4	15.77	<b>1</b>	<b>69.71</b>	<b>61.32</b>	<b>46.77</b>	<b>25.64</b>	15.86	<b>5</b>	<b>89.96</b>	<b>58.40</b>	14.33	6	<b>42.63</b>

SFT under various settings, demonstrating strong versatility across diverse domains. Please see Appendix G.6 for additional Math and Code results on GSM8K (Cobbe et al., 2021) and HumanEval (Chen et al., 2021a). Case studies are included in Appendix F.

**Gradient Stability.** While our theoretical analysis focuses on the variance of thought-level advantage estimation, its implications for optimization stability follow from the structure of the GRPO-MA objective in Eq. 2, where advantage estimates play a central role in shaping gradient updates. By reducing advantage variance through answer-level branching, GRPO-MA indirectly suppresses extreme gradient magnitudes and leads to more stable optimization. Consistent with this implication, T4A4 achieves the lowest GSS@10 in most experimental settings, indicating a substantially reduced frequency of gradient spikes during training. Additional grad\_norm and GSS curves are provided in Appendix G.5.

**Performance and Efficiency** We analyze efficiency from two complementary perspectives: (1) From a per-step sampling cost perspective, normalizing by the cost of T4A1 reveals a scaling pattern across tasks. Extending sampling along the answer dimension incurs only a modest increase in per-step wall-clock cost (typically on the order of  $1.1\text{--}1.3\times$  relative to T4A1), whereas increasing the number of independently sampled thoughts leads to a substantially larger computational overhead (approximately  $1.8\text{--}2.4\times$ ). Importantly, despite operating at a significantly lower per-step cost, answer-level branching (T4A4) consistently achieves

slightly better final performance than thought-scaling baselines (T16A1). (2) Beyond per-step cost, we further evaluate efficiency from an end-to-end wall-clock perspective. As shown by the wall-clock time curves in Appendix G.4, GRPO-MA reaches peak performance earlier than baselines and attains the highest final performance using less training time. This indicates that the improved optimization stability brought by reduced variance in thought-level advantage estimation not only avoids excessive per-step overhead in T16A1, but also accelerates effective progress during training in practice.

These results indicate that the efficiency gains of GRPO-MA do not arise from trading off performance for train speed. Instead, they stem from a more effective allocation of additional samples across sampling levels: by concentrating extra sampling on the answer dimension, GRPO-MA yields more stable advantage estimates, allowing improved optimization behavior to translate into both faster training and stronger performance. Crucially, this also implies that such gains cannot be achieved by expanding thought samples alone, rendering answer-level branching a necessary design choice for achieving reliable variance reduction and efficient optimization under GRPO-style training.

## 5.2. Simulator-based Manipulation Task

### 5.2.1. TASK SETTING

We largely follow the experimental protocol of ManipLLM (Li et al., 2024), a simulator-based framework for

## Why Tree-Style Branching Matters

Table 4. Combined Results for OCR-based VQA and Trajectory Prediction. TN: The number of thoughts; AN: The number of answers per thought; S/S: Second/Step during training. Bold indicates the best performance among models of the same size.

Model	TN	AN	OCR-based VQA				Trajectory Prediction						
			S/S	GSS@10	Infographics	St VQA	Doc VQA	S/S	GSS@10	DFD	HD	RMSE	EndPoint
Qwen2.5-VL-3B					73.10	67.63	91.33			571.60	537.63	404.40	429.93
Qwen2.5-VL-7B					78.94	74.03	93.51			496.44	451.19	340.33	354.03
Qwen2.5-VL-72B					79.72	74.27	93.26			386.83	352.18	263.61	300.77
SFT					74.77	69.68	92.94			277.68	261.86	196.55	228.62
GRPO	4	1	14.79	42	73.70	68.94	93.15	29.17	14	187.99	172.58	140.80	142.74
GRPO	8	1	19.62	88	76.33	71.56	93.98	34.51	18	172.41	157.09	130.09	137.29
GRPO	16	1	26.79	68	76.65	72.25	94.20	66.55	21	165.16	149.59	122.95	130.56
GRPO-MA	4	4	17.17	<b>17</b>	<b>76.69</b>	<b>72.48</b>	<b>94.22</b>	35.41	<b>10</b>	<b>151.10</b>	<b>138.29</b>	<b>111.59</b>	<b>120.60</b>

visual manipulation. To make the task more challenging, we introduce two changes. First, to increase observational diversity, the camera viewpoint is randomly sampled in each trial. Second, we adopt a stricter success criterion: an attempt is immediately counted as a failure if the predicted contact point is not on the target object surface. As in ManipLLM, when the model predicts a grasp point in the image, we execute a rule-based grasping routine. The suction cup approaches the predicted point along the local surface normal, and we further adjust the subsequent trajectory based on the object category. We evaluate performance by the success rate of predicted points that result in successful manipulation.

Table 5. Manipulating Point Prediction. TN: The number of thoughts; AN: The number of answers per thought; S/S: Second/Step during training.

Model	TN	AN	Success Rate (%)	
			Seen	Unseen
Qwen2.5-VL-3B			4.73%	1.30%
ManipLLM-7B			22.80%	7.63%
SFT			9.17%	4.28%
CoT-SFT			28.18%	11.79%
GRPO	4	1	10.75%	3.94%
GRPO-NoThink	0	16	10.60%	2.40%
GRPO-MA	4	4	<b>31.40%</b>	<b>16.00%</b>

### 5.2.2. BASELINES

We adapt some of the baselines used above and add several additional baselines. **ManipLLM-7B**: They collect a large number of successful samples in the simulator and constructs multiple task-specific question-answer pairs, utilizing the SFT training approach. We fine-tune their weights in the new settings. **CoT-SFT**: We collect successful samples of GRPO-MA-T4A4 (including the chain of thoughts and answers), then fine-tune Qwen2.5-VL-3B using SFT. **GRPO-NoThink**: We employ GRPO to train the Qwen2.5-VL-3B, but we do not require the model to generate a thought process; instead, it directly produces the answers.

### 5.2.3. MAIN RESULTS ON MANIPULATION TASK

Manipulation tasks with sparse rewards constitute an extreme high-variance regime for GRPO-style training<sup>2</sup>, where instability in thought-level advantage estimation is particularly pronounced. The experimental results are presented in Tab. 5. A direct comparison shows that T4A4 significantly outperforms T4A1, indicating that answer-level branching is especially effective in this setting by stabilizing training and facilitating the discovery of successful responses under sparse supervision. This result further supports our variance-based analysis, suggesting that tree-style branching becomes particularly important for reliable credit assignment in high-variance manipulation tasks.

### 5.3. More Baseline Comparison

Table 6. More Baseline Comparison on Trajectory Prediction .

Model	DFD	HD	RMSE	EP
GRPO	187.99	172.58	140.80	142.74
GRPO-CARE	188.23	170.82	139.83	144.85
DAPO	184.08	167.75	136.18	146.99
Dr.GRPO	180.56	165.95	135.86	140.05
TreeRPO-128	165.27	149.77	123.42	131.45
TreeRPO-64	157.03	144.52	113.99	125.08
<b>GRPO-MA</b>	<b>151.10</b>	<b>138.29</b>	<b>111.59</b>	<b>120.60</b>

To provide a broader comparison, we evaluate four recent GRPO-based variants—GRPO-CARE, DAPO, Dr.GRPO, and TreeRPO—on the trajectory prediction task. As shown in Table 6, GRPO-MA achieves the best performance across all metrics. GRPO-CARE, DAPO, and Dr.GRPO improve GRPO via loss or normalization refinements but do not introduce explicit branching, so thought-level advantages are still estimated from single outcomes and remain high-variance under sparse rewards. TreeRPO relies on token-

<sup>2</sup>For simplicity, we assume a binary reward  $R \in \{0, 1\}$  that follows a Bernoulli distribution with success probability  $p$ . When  $p$  is very small, reward observations are extremely noisy, making single-sample estimates unreliable and leading to high variance in thought-level advantage estimation.

length-based branching, where the suffix (*e.g.*, -64 or -128) denotes the maximum segment length used for splitting responses. As a result, its behavior is sensitive to response length: TreeRPO-128 degenerates to standard GRPO when responses are short, resulting in poorer performance compared to TreeRPO-64. Although TreeRPO-64 mitigates this issue and improves performance relative to TreeRPO-128, it still underperforms GRPO-MA, which we conjecture is due to higher-variance estimation of values (or advantages) for thoughts in sub-branches induced by branching at intermediate segments. In contrast, our XML-tag-based branching operates on semantic boundaries, enabling stable branching and reducing variance in thought-level advantage estimation across variable-length outputs.

#### 5.4. The Effectiveness on Larger Model Size

To study how GRPO-MA behaves as model capacity increases, we conduct a scaling experiment on Qwen2.5-VL-7B-Instruct. The 7B scale is a commonly used “large” checkpoint for tree-search- or multi-sampling-based reasoning methods (Guo et al., 2025; Kazemnejad et al., 2024; Li et al., 2025), offering a practical trade-off between model capacity and the computation required by expanded rollouts. We compare GRPO-MA with a matched GRPO baseline using identical training settings on the trajectory prediction task. Results are summarized in Table 7. Notably, GRPO-MA still outperforms GRPO, indicating that multi-answer sampling continue to benefit larger models.

Table 7. Qwen2.5-VL-7B-Instruct on Trajectory Prediction.

Model	DFD	HD	RMSE	EP
7B-T8A1	167.32	152.34	129.50	134.60
3B-MA-T4A4	151.10	138.29	111.59	120.60
<b>7B-MA-T8A4</b>	<b>134.67</b>	<b>121.89</b>	<b>103.64</b>	<b>103.27</b>

#### 5.5. The Effectiveness on Different Model Architecture

we evaluate GRPO-MA on the pure-text language model rather than a vision language model, Qwen3-4B-Instruct, for math and code reasoning tasks. The training settings remain the same as before. These results shown in Table 8 indicate that GRPO-MA continues to provide improvements even on pure text models, Qwen3-4B-Instruct, supporting the generality of our approach on different model architectures.

Table 8. Qwen3-4B-Instruct on Math and Code.

Model	Pass@1(N=10) on Math	Pass@1(N=10) on Code
GRPO-T4A1	17.53	4.22
<b>GRPO-MA-T4A4</b>	<b>18.07</b>	<b>6.25</b>

### 5.6. Ablation Study

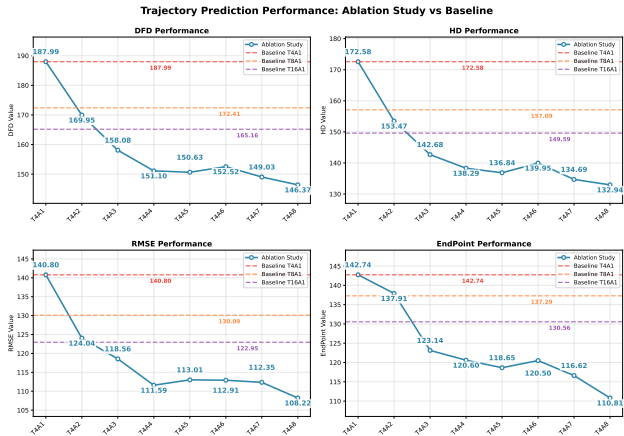


Figure 2. Ablation Study on Trajectory Prediction While maintaining the number of thoughts  $K = 4$ , we gradually increase the number of responses  $M$  per thought from 1 to 8 (*i.e.*, the number of responses is 4, 8, 12...32).

We conduct a detailed ablation study on the trajectory prediction task to analyze the effect of the number of answers per thought  $M$ , as shown in Fig. 2. The results indicate that as  $M$  increases, most evaluation metrics tend to decline, although the rate of decline becomes progressively smaller.

Surprisingly, T4A3 (4 thoughts, 12 answers) outperforms T16A1 (16 thoughts, 16 answers) across all metrics. A plausible reason is that thought quality matters more than reward-signal quantity: we score each thought by averaging the rewards of its  $M$  sampled answers,  $V(th_i) = \frac{1}{M} \sum_{j=1}^M R_{i,j}$ . With  $M = 3$ , T4A3 yields a more stable value estimate than T16A1’s single-sample evaluation ( $M = 1$ ), which is more sensitive to reward noise.

### 6. Conclusion

Under a simplified tree-branching setting where multiple answers are sampled per thought, we provide a variance-based analysis of thought-level advantage estimation in GRPO-style training. Our analysis reveals a fundamental asymmetry: increasing the number of answers per thought  $M$  monotonically decreases the variance toward zero, whereas increasing the number of sampled thoughts  $K$  leaves a strictly positive variance floor. Accordingly, under GRPO-style estimators without value models and absent additional mechanisms for controlling thought generation, multi-answer branching emerges as an effective and potentially necessary means for achieving stable and accurate advantage estimation. Empirically, GRPO-MA, a simple instantiation of this principle, consistently improves performance and optimization stability across different tasks, model configurations.

## Impact Statement

This paper presents work whose goal is to advance the field of Large Language Models. There are many potential societal consequences of our work, none of which we feel must be specifically highlighted here.

## References

- Bai, S., Chen, K., Liu, X., Wang, J., Ge, W., Song, S., Dang, K., Wang, P., Wang, S., Tang, J., et al. Qwen2. 5-vl technical report. *arXiv preprint arXiv:2502.13923*, 2025.
- Biten, A. F., Tito, R., Mafla, A., Gomez, L., Rusinol, M., Mathew, M., Jawahar, C., Valveny, E., and Karatzas, D. Icdar 2019 competition on scene text visual question answering. In *2019 International Conference on Document Analysis and Recognition (ICDAR)*, pp. 1563–1570. IEEE, 2019.
- Chen, M., Tworek, J., Jun, H., Yuan, Q., de Oliveira Pinto, H. P., Kaplan, J., Edwards, H., Burda, Y., Joseph, N., Brockman, G., Ray, A., Puri, R., Krueger, G., Petrov, M., Khlaaf, H., Sastry, G., Mishkin, P., Chan, B., Gray, S., Ryder, N., Pavlov, M., Power, A., Kaiser, L., Bavarian, M., Winter, C., Tillet, P., Such, F. P., Cummings, D., Plappert, M., Chantzis, F., Barnes, E., Herbert-Voss, A., Guss, W. H., Nichol, A., Paino, A., Tezak, N., Tang, J., Babuschkin, I., Balaji, S., Jain, S., Saunders, W., Hesse, C., Carr, A. N., Leike, J., Achiam, J., Misra, V., Morikawa, E., Radford, A., Knight, M., Brundage, M., Murati, M., Mayer, K., Welinder, P., McGrew, B., Amodei, D., McCandlish, S., Sutskever, I., and Zaremba, W. Evaluating large language models trained on code. 2021a.
- Chen, M., Tworek, J., Jun, H., Yuan, Q., Pinto, H. P. D. O., Kaplan, J., Edwards, H., Burda, Y., Joseph, N., Brockman, G., et al. Evaluating large language models trained on code. *arXiv preprint arXiv:2107.03374*, 2021b.
- Chen, Y., Ge, Y., Wang, R., Ge, Y., Cheng, J., Shan, Y., and Liu, X. Grpo-care: Consistency-aware reinforcement learning for multimodal reasoning. *arXiv preprint arXiv:2506.16141*, 2025.
- Chu, X., Huang, H., Zhang, X., Wei, F., and Wang, Y. Gpg: A simple and strong reinforcement learning baseline for model reasoning. *arXiv preprint arXiv:2504.02546*, 2025.
- Cobbe, K., Kosaraju, V., Bavarian, M., Chen, M., Jun, H., Kaiser, L., Plappert, M., Tworek, J., Hilton, J., Nakano, R., Hesse, C., and Schulman, J. Training verifiers to solve math word problems. *arXiv preprint arXiv:2110.14168*, 2021.
- contributors, A. W. C. Agibot world colosseum. <https://github.com/OpenDriveLab/Agibot-World>, 2024.
- Eiter, T., Mannila, H., et al. Computing discrete fréchet distance. 1994.
- Feng, K., Gong, K., Li, B., Guo, Z., Wang, Y., Peng, T., Wu, J., Zhang, X., Wang, B., and Yue, X. Video-r1: Reinforcing video reasoning in mllms. *arXiv preprint arXiv:2503.21776*, 2025.
- Guo, Y., Xu, L., Liu, J., Ye, D., and Qiu, S. Segment policy optimization: Effective segment-level credit assignment in rl for large language models. *arXiv preprint arXiv:2505.23564*, 2025.
- Hou, Z., Hu, Z., Li, Y., Lu, R., Tang, J., and Dong, Y. Treerl: Llm reinforcement learning with on-policy tree search. *arXiv preprint arXiv:2506.11902*, 2025.
- Hu, E. J., Shen, Y., Wallis, P., Allen-Zhu, Z., Li, Y., Wang, S., Wang, L., Chen, W., et al. Lora: Low-rank adaptation of large language models. *ICLR*, 1(2):3, 2022.
- Huang, T., Zhu, Z., Jin, G., Liu, L., Wang, Z., and Liu, S. Spam: Spike-aware adam with momentum reset for stable llm training. *arXiv preprint arXiv:2501.06842*, 2025a.
- Huang, W., Jia, B., Zhai, Z., Cao, S., Ye, Z., Zhao, F., Xu, Z., Hu, Y., and Lin, S. Vision-r1: Incentivizing reasoning capability in multimodal large language models. *arXiv preprint arXiv:2503.06749*, 2025b.
- Huttenlocher, D. P., Klanderman, G. A., and Rucklidge, W. J. Comparing images using the hausdorff distance. *IEEE Transactions on pattern analysis and machine intelligence*, 15(9):850–863, 2002.
- Ji, Y., Tan, H., Shi, J., Hao, X., Zhang, Y., Zhang, H., Wang, P., Zhao, M., Mu, Y., An, P., et al. Robobrain: A unified brain model for robotic manipulation from abstract to concrete. In *Proceedings of the Computer Vision and Pattern Recognition Conference*, pp. 1724–1734, 2025.
- Kazemnejad, A., Aghajohari, M., Portelance, E., Sordoni, A., Reddy, S., Courville, A., and Le Roux, N. Vineppo: Unlocking rl potential for llm reasoning through refined credit assignment. 2024.
- Khanna, M., Mao, Y., Jiang, H., Haresh, S., Shacklett, B., Batra, D., Clegg, A., Undersander, E., Chang, A. X., and Savva, M. Habitat synthetic scenes dataset (hssd-200): An analysis of 3d scene scale and realism tradeoffs for objectgoal navigation. In *Proceedings of the IEEE/CVF Conference on Computer Vision and Pattern Recognition*, pp. 16384–16393, 2024.

- Kim, D., Park, S., Jang, H., Shin, J., Kim, J., and Seo, Y. Robot-r1: Reinforcement learning for enhanced embodied reasoning in robotics. *arXiv preprint arXiv:2506.00070*, 2025.
- Li, X., Zhang, M., Geng, Y., Geng, H., Long, Y., Shen, Y., Zhang, R., Liu, J., and Dong, H. Manipllm: Embodied multimodal large language model for object-centric robotic manipulation. In *Proceedings of the IEEE/CVF Conference on Computer Vision and Pattern Recognition*, pp. 18061–18070, 2024.
- Li, Y., Gu, Q., Wen, Z., Li, Z., Xing, T., Guo, S., Zheng, T., Zhou, X., Qu, X., Zhou, W., et al. Treepo: Bridging the gap of policy optimization and efficacy and inference efficiency with heuristic tree-based modeling. *arXiv preprint arXiv:2508.17445*, 2025.
- Liu, Z., Chen, C., Li, W., Qi, P., Pang, T., Du, C., Lee, W. S., and Lin, M. Understanding r1-zero-like training: A critical perspective. *arXiv preprint arXiv:2503.20783*, 2025.
- Luo, H., Zhai, W., Zhang, J., Cao, Y., and Tao, D. Learning affordance grounding from exocentric images. In *Proceedings of the IEEE/CVF conference on computer vision and pattern recognition*, pp. 2252–2261, 2022.
- Maxwell-Jia. Aime2024. [https://huggingface.co/datasets/Maxwell-Jia/AIME\\_2024](https://huggingface.co/datasets/Maxwell-Jia/AIME_2024), 2024.
- Myers, A., Teo, C. L., Fermüller, C., and Aloimonos, Y. Affordance detection of tool parts from geometric features. In *ICRA*, 2015.
- PrimeIntellect. Synthetic-1: Scaling distributed synthetic data generation for verified reasoning. <https://www.primeintellect.ai/blog/synthetic-1>, 2024.
- Schulman, J., Wolski, F., Dhariwal, P., Radford, A., and Klimov, O. Proximal policy optimization algorithms. *arXiv preprint arXiv:1707.06347*, 2017.
- Shao, Z., Wang, P., Zhu, Q., Xu, R., Song, J., Bi, X., Zhang, H., Zhang, M., Li, Y., et al. Deepseekmath: Pushing the limits of mathematical reasoning in open language models. *arXiv preprint arXiv:2402.03300*, 2024.
- Shen, H., Liu, P., Li, J., Fang, C., Ma, Y., Liao, J., Shen, Q., Zhang, Z., Zhao, K., Zhang, Q., et al. Vlm-r1: A stable and generalizable r1-style large vision-language model. *arXiv preprint arXiv:2504.07615*, 2025.
- Simoni, M., Fontana, A., Rossolini, G., and Saracino, A. Gtpo: Trajectory-based policy optimization in large language models. *arXiv preprint arXiv:2508.03772*, 2025.
- Song, Z., Ouyang, G., Li, M., Ji, Y., Wang, C., Xu, Z., Zhang, Z., Zhang, X., Jiang, Q., Chen, Z., et al. Manipvlm-r1: Reinforcement learning for reasoning in embodied manipulation with large vision-language models. *arXiv preprint arXiv:2505.16517*, 2025.
- Tito, R., Mathew, M., Jawahar, C., Valveny, E., and Karatzas, D. Icdar 2021 competition on document visual question answering. In *International Conference on Document Analysis and Recognition*, pp. 635–649. Springer, 2021.
- Wang, H., Liu, P., Cai, W., Wu, M., Qian, Z., and Dong, H. Mo-ddn: A coarse-to-fine attribute-based exploration agent for multi-object demand-driven navigation. *Advances in Neural Information Processing Systems*, 37: 64176–64214, 2024.
- White, C., Dooley, S., Roberts, M., Pal, A., Feuer, B., Jain, S., Shwartz-Ziv, R., Jain, N., Saifullah, K., Naidu, S., et al. Livebench: A challenging, contamination-free llm benchmark. *arXiv preprint arXiv:2406.19314*, 4, 2024.
- Xiang, F., Qin, Y., Mo, K., Xia, Y., Zhu, H., Liu, F., Liu, M., Jiang, H., Yuan, Y., Wang, H., Yi, L., Chang, A. X., Guibas, L. J., and Su, H. SAPIEN: A simulated part-based interactive environment. In *The IEEE Conference on Computer Vision and Pattern Recognition (CVPR)*, June 2020.
- Yang, Z., Guo, Z., Huang, Y., Liang, X., Wang, Y., and Tang, J. Treerpo: Tree relative policy optimization. *arXiv preprint arXiv:2506.05183*, 2025.
- Yu, Q., Zhang, Z., Zhu, R., Yuan, Y., Zuo, X., Yue, Y., Dai, W., Fan, T., Liu, G., Liu, L., et al. Dapo: An open-source llm reinforcement learning system at scale. *arXiv preprint arXiv:2503.14476*, 2025.
- Zhao, Y., Liu, Y., Liu, J., Chen, J., Wu, X., Hao, Y., Lv, T., Huang, S., Cui, L., Ye, Q., et al. Geometric-mean policy optimization. *arXiv preprint arXiv:2507.20673*, 2025.
- Zheng, C., Liu, S., Li, M., Chen, X.-H., Yu, B., Gao, C., Dang, K., Liu, Y., Men, R., Yang, A., et al. Group sequence policy optimization. *arXiv preprint arXiv:2507.18071*, 2025.

## A. Appendix Outline

Below is the table of contents for the appendix.

- More Related Work [B](#)
- Full Analysis of Variance [C](#)
  - The Multivariate Delta Method [C.1](#)
  - Asymptotic Normality of the Estimated Value Vector [C.2](#)
  - Application to the Thought Advantage Function [C.3](#)
  - Application to the Answer Advantage Function [C.4](#)
  - Diagonality Analysis of Matrices [C.5](#)
- Details in Task Settings [D](#)
  - Math [D.1](#)
  - Code [D.2](#)
  - Object Detection [D.3](#)
  - Affordance Prediction [D.4](#)
  - Trajectory Prediction [D.5](#)
  - Demand Prediction [D.6](#)
  - Ocr-based VQA [D.7](#)
  - Simulator-based Visual Manipulation [D.8](#)
- Details in Training [E](#)
  - Training Hyperparameters [E.1](#)
  - SFT Details [E.2](#)
  - Generation Configure [E.3](#)
- Case Study and Visualization [F](#)
- More Experimental Analysis [G](#)
  - Inconsistency Analysis [G.1](#)
  - Accuracy Reward Curve [G.2](#)
  - Richness of Reward Signal [G.3](#)
  - Wall-clock Time [G.4](#)
  - Grad-norm and GSS Curve [G.5](#)
  - More Results on Code and Math [G.6](#)
- Usage of LLMs [H](#)

## B. More Related Work: Applications of GRPO in Multimodal Domains

VLM-R1 (Shen et al., 2025) applies a general GRPO pipeline to Vision-Language Models, enabling smaller models to achieve competitive performance on complex visual reasoning tasks. Vision-R1 (Huang et al., 2025b) generates high-quality multimodal Chain-of-Thought data and uses Progressive Thinking Suppression Training (PTST) to prevent the model from creating overly long reasoning paths. Video-R1 (Feng et al., 2025) introduces Temporal-GRPO (T-GRPO), a novel reward scheme that encourages the model to leverage temporal information in video sequences. ManipLVM-R1 (Song et al., 2025) employs GRPO for robotic manipulation with new affordance-aware and trajectory matching reward functions to improve the localization of interactive parts and the physical plausibility of actions. Robot-R1 (Kim et al., 2025) reframes robot learning as a multiple-choice question answering task, using GRPO to optimize the reasoning for embodied manipulation.

## C. Full Analysis of Variance

This section provides a full derivation of the approximate variance for the Thought Advantage,  $A(th_i)$ , as presented in the main paper. We first review the multivariate Delta Method, establish the asymptotic normality of our estimators via the Central Limit Theorem (CLT), and finally present the detailed application and gradient calculation.

### C.1. The Multivariate Delta Method

The Delta Method is a fundamental result in statistics used to approximate the moments of a function of one or more random variables. The multivariate version is central to our analysis.

**General Formulation.** Let  $\vec{V} = (V_1, V_2, \dots, V_K)$  be a  $K$ -dimensional random vector of estimators with a true mean vector  $\vec{\mu} = (\mu_1, \mu_2, \dots, \mu_K)$ . Let  $M$  denote the sample size used to compute each estimator  $V_k$ . To emphasize that these estimators are functions of the sample size, we denote the vector as  $\vec{V}_M$ . The Delta Method provides the asymptotic distribution of  $f(\vec{V}_M)$  as  $M \rightarrow \infty$ . Specifically, if  $\vec{V}_M$  satisfies the condition for the Central Limit Theorem such that:

$$\sqrt{M}(\vec{V}_M - \vec{\mu}) \xrightarrow{d} N(0, \Sigma_{\text{asymptotic}}) \quad (4)$$

where  $\xrightarrow{d}$  denotes convergence in distribution, then the transformed variable  $f(\vec{V}_M)$  also converges in distribution:

$$\sqrt{M}(f(\vec{V}_M) - f(\vec{\mu})) \xrightarrow{d} N(0, \nabla f(\vec{\mu})^T \Sigma_{\text{asymptotic}} \nabla f(\vec{\mu})) \quad (5)$$

From this formal result, we derive the practical formula for approximating the variance of  $f(\vec{V}_M)$  for a large but finite sample size  $M$ . The term  $\sqrt{M}$  acts as a scaling factor that ensures the limiting distribution has a finite, non-zero variance. The variance of the estimator itself is given by:

$$\text{Var}(f(\vec{V}_M)) \approx \nabla f(\vec{\mu})^T \text{Var}(\vec{V}_M) \nabla f(\vec{\mu}) \quad (6)$$

where  $\text{Var}(\vec{V}_M)$  is the actual covariance matrix of the estimator vector, which is related to the asymptotic covariance by  $\text{Var}(\vec{V}_M) \approx \Sigma_{\text{asymptotic}}/M$ .

### C.2. Asymptotic Normality of the Estimated Value Vector

Before applying the Delta Method, we must first establish that our core estimator, the vector of estimated values  $\vec{V}(th)$ , satisfies the prerequisite of being asymptotically normal. This justification comes from the Central Limit Theorem (CLT).

For each thought  $th_k$ , its estimated value  $V(th_k)$  is the sample mean of  $M$  i.i.d. random variables, the rewards  $\{R_{k,j}\}_{j=1}^M$ :

$$V(th_k) = \frac{1}{M} \sum_{j=1}^M R_{k,j} \quad (7)$$

The rewards have a finite true mean  $\mu_{R_k}$  and a finite true variance  $\sigma_{R_k}^2$ . According to the CLT, as the sample size  $M \rightarrow \infty$ , the distribution of the standardized sample mean converges to a normal distribution. This is formally stated as:

$$\sqrt{M}(V(th_k) - \mu_{R_k}) \xrightarrow{d} N(0, \sigma_{R_k}^2) \quad (8)$$

We now extend this to the full  $K$ -dimensional vector of estimators,  $\vec{V}(th) = (V(th_1), \dots, V(th_K))$ . Since we have assumed that the estimated values for different thoughts are mutually independent, the joint asymptotic distribution of the vector is also normal. The mean of this limiting distribution is a zero vector, and the covariance matrix is diagonal, composed of the individual variances. Therefore, the entire vector of estimators is asymptotically normal:

$$\sqrt{M}(\vec{V}(th) - \vec{\mu}) \xrightarrow{d} N(0, \Sigma_{\text{diag}}) \quad (9)$$

where  $\vec{\mu} = (\mu_{R_1}, \dots, \mu_{R_K})$  is the vector of true means, and  $\Sigma_{\text{diag}}$  is the diagonal covariance matrix of the limiting distribution:

$$\Sigma_{\text{diag}} = \begin{pmatrix} \sigma_{R_1}^2 & 0 & \cdots & 0 \\ 0 & \sigma_{R_2}^2 & \cdots & 0 \\ \vdots & \vdots & \ddots & \vdots \\ 0 & 0 & \cdots & \sigma_{R_K}^2 \end{pmatrix} \quad (10)$$

This result formally justifies the application of the Multivariate Delta Method to the thought advantage function  $A(th_i) = f_i(\overrightarrow{V(th)})$ .

### C.3. Application to the Thought Advantage Function

**Verification of Assumptions.** The prerequisites for the Delta Method are satisfied. First, as established above, our estimator vector  $\overrightarrow{V(th)}$  is asymptotically normal. Second, the advantage function  $A(th_i) = (V(th_i) - \bar{V})/S_V$  is continuously differentiable everywhere except where the denominator  $S_V = 0$ , where  $\bar{V} = \frac{1}{K} \sum_{k=1}^K V(th_k)$  and  $S_V = \sqrt{\frac{1}{K-1} \sum_{k=1}^K (V(th_k) - \bar{V})^2}$ . We evaluate the gradient at  $\vec{\mu}$ , where the denominator's analogue is  $\sigma_{\mu_R}$ . The approximation is thus valid assuming  $\sigma_{\mu_R} > 0$ , *i.e.*, not all thoughts have the same true value.

**Gradient Calculation.** Let  $\overrightarrow{V(th)} = V = (V_1, \dots, V_K)$  and define

$$f_i(V) = A(th_i) = \frac{N_i(V)}{D(V)} = \frac{V_i - \bar{V}}{S_V}, \quad \bar{V} = \frac{1}{K} \sum_{j=1}^K V_j,$$

$$Q(V) = \frac{1}{K-1} \sum_{j=1}^K (V_j - \bar{V})^2, \quad D(V) = S_V = \sqrt{Q(V)}.$$

We compute  $\partial f_i / \partial V_k$  in steps.

First,

$$\frac{\partial \bar{V}}{\partial V_k} = \frac{1}{K}, \quad \frac{\partial N_i}{\partial V_k} = \delta_{ik} - \frac{1}{K}. \quad (11)$$

For  $Q$  we have, using  $\partial(V_j - \bar{V}) / \partial V_k = \delta_{jk} - \frac{1}{K}$ ,

$$\frac{\partial Q}{\partial V_k} = \frac{1}{K-1} \sum_{j=1}^K 2(V_j - \bar{V})(\delta_{jk} - \frac{1}{K}) \quad (12)$$

$$= \frac{2}{K-1} \left[ (V_k - \bar{V}) - \frac{1}{K} \sum_{j=1}^K (V_j - \bar{V}) \right] = \frac{2}{K-1} (V_k - \bar{V}), \quad (13)$$

because  $\sum_j (V_j - \bar{V}) = 0$ . Therefore

$$\frac{\partial D}{\partial V_k} = \frac{1}{2D} \frac{\partial Q}{\partial V_k} = \frac{V_k - \bar{V}}{(K-1)D}. \quad (14)$$

Applying the quotient rule yields, for arbitrary  $V$ ,

$$\frac{\partial f_i}{\partial V_k} = \frac{(\delta_{ik} - \frac{1}{K})D - (V_i - \bar{V}) \cdot \frac{V_k - \bar{V}}{(K-1)D}}{D^2} = \frac{\delta_{ik} - \frac{1}{K}}{D} - \frac{(V_i - \bar{V})(V_k - \bar{V})}{(K-1)D^3}. \quad (15)$$

Evaluate at  $V = \vec{\mu}$  and denote

$$\sigma_{\mu_R} := D|_{V=\mu} = \sqrt{\frac{1}{K-1} \sum_j (\mu_j - \bar{\mu})^2}, \quad \tilde{\mu}_j := \frac{\mu_j - \bar{\mu}}{\sigma_{\mu_R}}.$$

Then

$$\left. \frac{\partial f_i}{\partial V_k} \right|_{V=\mu} = \frac{1}{\sigma_{\mu_R}} \left( \delta_{ik} - \frac{1}{K} - \frac{\tilde{\mu}_i \tilde{\mu}_k}{K-1} \right). \quad (16)$$

Finally, by the first-order multivariate Delta method, with  $\text{Var}(\vec{V}) = \frac{1}{M} \Sigma_{\text{diag}}$  (and  $\Sigma_{\text{diag}} = \text{diag}(\sigma_{R_1}^2, \dots, \sigma_{R_K}^2)$ ),

$$\text{Var}[A(th_i)] \approx \nabla_V f_i(\mu)^\top \text{Var}(\vec{V}) \nabla_V f_i(\mu) = \frac{1}{M \sigma_{\mu_R}^2} \sum_{k=1}^K \left( \delta_{ik} - \frac{1}{K} - \frac{\tilde{\mu}_i \tilde{\mu}_k}{K-1} \right)^2 \sigma_{R_k}^2. \quad (17)$$

#### C.4. Application to the Answer Advantage Function

For a single answer  $ans_{i,j}$ , the advantage is defined as

$$A(ans_{i,j}) = \frac{R_{i,j} - \bar{R}}{S_R}, \quad \bar{R} = \frac{1}{KM} \sum_{k=1}^K \sum_{m=1}^M R_{k,m}, \quad S_R = \sqrt{\frac{1}{KM-1} \sum_{k=1}^K \sum_{m=1}^M (R_{k,m} - \bar{R})^2}. \quad (18)$$

Using the first-order multivariate Delta method, the variance of  $A(ans_{i,j})$  can be approximated as

$$\text{Var}[A(ans_{i,j})] \approx \nabla_{\mathbf{R}} g_{i,j}(\boldsymbol{\mu})^\top \text{diag}(\sigma_{R_1}^2, \dots, \sigma_{R_K}^2, \dots) \nabla_{\mathbf{R}} g_{i,j}(\boldsymbol{\mu}), \quad (19)$$

where  $g_{i,j}(\mathbf{R}) = A(ans_{i,j})$  and  $\boldsymbol{\mu}$  denotes the vector of reward means.

Evaluating the gradient at  $\mathbf{R} = \boldsymbol{\mu}$  and grouping by thought, we obtain

$$\text{Var}[A(ans_{i,j})] \approx \frac{KM-1}{M(K-1)\sigma_{\mu_R}^2} \sum_{k=1}^K \sum_{m=1}^M \left( \delta_{(k,m),(i,j)} - \frac{1}{KM} - \frac{\tilde{\mu}_i \tilde{\mu}_k}{M(K-1)} \right)^2 \sigma_{R_k}^2, \quad (20)$$

where  $\delta_{(k,m),(i,j)}$  is the Kronecker delta,  $\tilde{\mu}_k = (\mu_{R_k} - \mu_{\bar{R}})/\sigma_{\mu_R}$  is the expected advantage of thought  $th_k$ ,  $\mu_{\bar{R}} = \frac{1}{K} \sum_{k=1}^K \mu_{R_k}$ , and  $\sigma_{\mu_R}^2 = \frac{1}{K-1} \sum_{k=1}^K (\mu_{R_k} - \mu_{\bar{R}})^2$ .

#### C.5. Diagonality Analysis of Matrices

To examine whether the assumption of independence across thoughts (*i.e.*, a diagonal covariance matrix) holds in practice, we conducted numerical simulations and empirically estimated the covariance structure of  $\vec{V}(th) = (V_1, \dots, V_K)$ . Specifically, we generated  $N$  independent replications of the full  $K$ -dimensional estimator vector, denoted  $V^{(n)}$  for  $n = 1, \dots, N$ , and computed the empirical covariance matrix:

$$\hat{\Sigma} = \frac{1}{N-1} \sum_{n=1}^N (V^{(n)} - \bar{V})(V^{(n)} - \bar{V})^\top, \quad \bar{V} = \frac{1}{N} \sum_{n=1}^N V^{(n)}. \quad (21)$$

We then assessed the degree of diagonal dominance using Row-wise strict diagonal dominance and Frobenius-norm based diagonal energy ratio.

**Row-wise strict diagonal dominance.** For each row  $i$ , the covariance matrix is said to be strictly diagonally dominant if

$$|\hat{\Sigma}_{ii}| > \sum_{j \neq i} |\hat{\Sigma}_{ij}|. \quad (22)$$

We summarize this property by the proportion of rows that satisfy the condition:

$$p_{\text{row\_dom}} = \frac{1}{K} \sum_{i=1}^K \mathbf{1} \left\{ |\hat{\Sigma}_{ii}| > \sum_{j \neq i} |\hat{\Sigma}_{ij}| \right\}, \quad (23)$$

where  $\mathbf{1}\{\cdot\}$  denotes the indicator function. A value  $p_{\text{row\_dom}} \approx 1$  indicates strong diagonal dominance.

**Frobenius-norm based diagonal energy ratio.** We also consider the proportion of squared Frobenius norm explained by the diagonal entries:

$$\rho_F = \frac{\sum_{i=1}^K \hat{\Sigma}_{ii}^2}{\sum_{i=1}^K \sum_{j=1}^K \hat{\Sigma}_{ij}^2}, \quad 0 \leq \rho_F \leq 1. \quad (24)$$

Higher values of  $\rho_F$  indicate that the diagonal terms dominate the overall covariance energy.

We select 50 samples from the Trajectory Prediction task and, at the 1500-step checkpoint, compute the covariance matrix of the thought-value estimates by performing  $N = 10$  independent replications per sample. The empirical results yield  $p_{\text{row\_dom}} = \mathbf{63.65\%}$  and  $\rho_F = \mathbf{70.71\%}$  averaged on 50 samples. Since our theoretical derivations rely on the assumption that the covariance matrix is diagonal, these diagnostics suggest that this assumption has a certain degree of validity in practice, as the estimated covariance matrices exhibit a clear tendency toward diagonal dominance.

## D. Details in Task Settings

### D.1. Math

We conduct our experiments using problems from the DAPO (Yu et al., 2025) training set and evaluate on the AIME2024 test set (Maxwell-Jia, 2024). The Math training set is constructed by randomly sampling 1,000 problems from the DAPO training corpus. The model is trained for a single epoch on these 1,000 training samples. We do not use a validation set; instead, we select the final model parameters saved at the end of training (the last checkpoint) for testing.

At test time, for each test problem from AIME2024 we generate  $n = 100$  independent candidate outputs (“generations”). From these 100 generations we compute the  $\text{pass}@k$  metrics for  $k \in \{10, 32\}$ .

The reward function is designed with two complementary components: a *format reward* and an *accuracy reward*. The model is required to generate outputs in a predefined structured format:

```
<analysis> xxx </analysis>
<process> xxx </process>
<answer> d </answer>
```

where the answer is represented as a single integer  $d$ . The format reward assigns a value of 1 if and only if the output strictly follows the required format, and 0 otherwise. The accuracy reward is +1 if the predicted answer is identical to the true answer, and 0 otherwise.

The full prompt template is shown below:

```
{Question} You MUST structure your response using exactly
threesections with XML-style tags in this exact order:
1) <analysis> ... </analysis>
2) <process> ... </process>
3) <answer> ... </answer>
```

Roles and constraints:

- <analysis>: State relevant concepts, theorems, formulas, and solution plan. Do NOT perform numeric calculations or write equations here.
- <process>: Perform ALL detailed computations and step-by-step derivations based on the analysis. Show equations and numeric work here.
- <answer>: Output ONLY the final integer (optional sign). No words, units, punctuation (except the sign), or explanations.

Hard requirements:

- All three tags must be present and appear in the exact

- order <analysis> -> <process> -> <answer>.
- No calculations in <analysis>.
- All computations must be in <process>.
- <answer> must contain a single integer only.

**Implementation Note:** In our multi-sample framework, the sampled content encompasses both < answer > and < process > elements.

### D.2. Code

We conduct our experiments using the Python-code portion of the SYNTHETIC-1 dataset (PrimeIntellect, 2024) and evaluate on the LiveBench code test set (White et al., 2024). The Code training set is constructed by randomly sampling 1,000 problems from the SYNTHETIC-1 Python-code corpus. The model is trained for a single epoch on these 1,000 training samples. We do not use a validation set; instead, we select the final model parameters saved at the end of training (the last checkpoint) for testing.

At test time, for each test problem from LiveBench we generate  $n = 100$  independent candidate outputs (“generations”). From these 100 generations we compute the  $pass@k$  metrics for  $k \in \{10, 32\}$  as described below.

The reward function is designed with two complementary components: a *format reward* and a *functional (accuracy) reward*. The model is required to generate outputs in a predefined structured format:

```
<think> xxx </think>
<answer> xxx </answer>
```

The format reward assigns a value of 1 if and only if the output strictly follows the required tag structure and the content within <answer> can be parsed as a syntactically valid Python program. Otherwise the format reward is 0.

The functional (accuracy) reward is +1 if the program inside <answer> executes successfully on the official hidden test inputs, terminates without runtime error, and produces outputs that exactly match the expected outputs for all test cases. Otherwise the accuracy reward is 0.

The prompt used to condition the model for each problem is exactly:

```
{Question} First output the thinking process in<think> </think> tags and
then output the final code in <answer> </answer> tags. The answer should
be a complete Python code solution that solves the given problem. Make
sure your code handles all edge cases and follows the input/output format
specified in the problem. DONOT OUTPUT ANY CODE OR SOLUTION IN THE THINK
TAGS.
```

### D.3. Object Detection

We conduct our experiments using the **Agibot World dataset** (contributors, 2024). The data is partitioned into training, validation, and test sets based on specific `task_ids` from Agibot World dataset. Specifically, the training set is constructed from `task_ids` 424, 480, and 507, comprising a total of 3,000 images (randomly sampling). The validation and test sets are derived from `task_id` 582 and 1352, respectively. For all images, the ground-truth bounding boxes and corresponding object labels are annotated through a crowdsourcing process. The object detection model is trained for a single epoch on the 3,000-image training set.

After training, we perform model selection by evaluating checkpoints on the designated validation set. The model checkpoint that achieves the highest average IoU@0.5 (as defined below) on the validation data is selected for the final evaluation. The performance of this selected model is then reported on the test set.

We evaluate the model’s performance using a **IoU rate** metric, which measures the proportion of correctly localized objects based on the Intersection over Union (IoU). A detection is considered positive if the IoU between the predicted bounding box ( $B_{pred}$ ) and the ground-truth bounding box ( $B_{gt}$ ) exceeds a given threshold  $\tau$ .

The IoU rate at a specific threshold  $\tau$ , denoted as  $\text{IoU}@_\tau$ , is formulated as:

$$\text{IoU}@_\tau = \frac{\sum_{i=1}^N \mathbb{I}(\text{IoU}(B_{\text{pred}}^{(i)}, B_{\text{gt}}^{(i)}) > \tau)}{N} \quad (25)$$

where  $N$  is the total number of samples in the test set, and  $\mathbb{I}(\cdot)$  is the indicator function. To provide a comprehensive assessment, we report the performance across four different IoU thresholds:  $\tau \in \{0.5, 0.6, 0.7, 0.8\}$ .

The reward function is designed with two complementary components: a *format reward* and an *accuracy reward*. The model is required to generate outputs in a predefined structured format:

```
<think> xxx </think>
<answer> [d, d, d, d] </answer>
```

where the bounding box is represented as a list of four integers  $[d, d, d, d]$ . The format reward assigns a value of 1 if and only if the output strictly follows the required format, and 0 otherwise. The accuracy reward is defined as the IoU between the predicted bounding box and the ground-truth bounding box.

The full prompt template is shown below:

```
{Question} First output the thinking process in <think> </think> tags and then
output the final answer in <answer> </answer> tags. Output the final answer in
List format. Only output the bounding box using [x_min, y_min, x_max, y_max] format
in the final answer. DO NOT OUTPUT ANY ANSWER OR CONCLUSION IN THE THINK TAGS.
```

#### D.4. Affordance Prediction

The task is defined as affordance prediction, where the model, given an image and a specified affordance (e.g., grasping, holding), is required to predict a pixel-wise mask indicating the corresponding region.

We primarily use the UMD Part Affordance Dataset (Myers et al., 2015). The official training split of this dataset is used to construct our training and validation sets. Specifically, we use 3,000 images for training and a held-out portion of the original training split for validation. For evaluation, we use the official test split of the UMD dataset. To further assess the model’s generalization capabilities, we also use the entire AGD20K dataset (Luo et al., 2022) as an additional, challenging test set.

The affordance prediction model is trained for a single epoch on the 3,000-image training set. After training, we perform model selection by evaluating checkpoints on the designated validation set. The model checkpoint that achieves the highest Success Rate (as defined below) on the validation data is selected for the final evaluation. The performance of this selected model is then reported on the test sets (UMD test and AGD20K).

We evaluate the model’s performance using a Success Rate metric. This metric measures the proportion of samples where the predicted point correctly falls within the ground-truth affordance mask. A prediction is considered successful if the pixel value at the predicted 2D coordinate is 1 in the ground-truth binary mask.

The Success Rate is formulated as:

$$\text{Success Rate} = \frac{\sum_{i=1}^N \mathbb{I}(M_{\text{gt}}^{(i)}(C_{\text{pred}}^{(i)}) = 1)}{N} \quad (26)$$

where  $N$  is the total number of samples in the test set,  $C_{\text{pred}}^{(i)}$  is the predicted 2D coordinate  $(x, y)$  for the  $i$ -th sample, and  $M_{\text{gt}}^{(i)}$  is the corresponding ground-truth affordance mask. The notation  $M_{\text{gt}}^{(i)}(C_{\text{pred}}^{(i)})$  represents the value of the mask at the predicted coordinate.  $\mathbb{I}(\cdot)$  is the indicator function, which is 1 if the condition is true and 0 otherwise.

The reward function consists of two complementary components: a *format reward* and an *accuracy reward*.

The model is required to generate outputs in the following structured format:

```
<think> xxx </think>
<answer> [d, d] </answer>
```

where the final answer corresponds to a 2D coordinate  $[d, d]$ , with  $d$  denoting an integer. The format reward assigns a value of 1 if and only if the output strictly adheres to this format; otherwise, it is set to 0. The accuracy reward evaluates the correctness of the prediction by checking whether the predicted 2D point lies within the ground-truth affordance mask (i.e., a region where the mask value equals 1). If the prediction falls inside the valid region, +1 reward is given; otherwise, it is not.

The full prompt template is shown below:

```
{Question} First output the thinking process in <think> </think> tags and then
output the final answer in <answer> </answer> tags. Only output one affordance
point using [x, y] format. DO NOT OUTPUT ANY ANSWER OR CONCLUSION IN THE THINK
TAGS.
```

### D.5. Trajectory Prediction

The task is defined as trajectory prediction, where the model, given an image and a manipulation instruction, is required to predict the two-dimensional trajectory of the robotic arm’s end-effector in the image’s pixel coordinate system. The trajectory is represented as a sequence of coordinates, and the predicted path should follow the ground-truth trajectory to successfully complete the instructed manipulation.

We primarily use the trajectory subset of the BAAI ShareRobot dataset (Ji et al., 2025). The original dataset is partitioned into training, validation, and test sets. Specifically, we use 3,000 images for training, a held-out portion of the training split for validation, and the test split for evaluation. The model is trained for a single epoch on the 3,000-image training set. After training, we perform model selection by evaluating checkpoints on the designated validation set. The checkpoint that achieves the highest reward value (as defined below) on the validation data is selected for the final evaluation. The performance of this selected model is then reported on the held-out test set.

We evaluate the model’s performance using multiple geometric similarity metrics, following the design in ManipVLM-R1 (Song et al., 2025). These metrics measure how well the predicted trajectory matches the ground truth from different perspectives. Specifically, we use Discrete Fréchet Distance (DFD), Hausdorff Distance (HD), Root Mean Square Error (RMSE), and Endpoint Distance as evaluation criteria.

The model is required to generate outputs in the following structured format:

```
<think> xxx </think>
<answer> [[x1, y1], [x2, y2], ..., [xn, yn]] </answer>
```

where the final answer corresponds to a variable-length sequence of 2D coordinates  $[x, y]$ , with  $x$  and  $y$  denoting integers.

The reward function consists of two complementary components: a *format reward* and a *accuracy reward*. The format reward assigns a value of 1 if and only if the output strictly adheres to this format; otherwise, it is set to 0. To measure how well the predicted trajectory  $\hat{T}$  matches the ground-truth trajectory  $T^*$ , we adopt an accuracy reward following the design in ManipVLM-R1 (Song et al., 2025). Specifically, the reward is defined as

$$R_{\text{acc}} = \exp(-k D_{\text{DFD}}(\hat{T}, T^*)) + \exp(-k D_{\text{HD}}(\hat{T}, T^*)) + \exp(-k D_{\text{RMSE}}(\hat{T}, T^*)) + \exp(-k \|\hat{p}_N - p_M^*\|^2), \tag{27}$$

where  $D_{\text{DFD}}$ ,  $D_{\text{HD}}$ , and  $D_{\text{RMSE}}$  denote the Discrete Fréchet Distance, Hausdorff Distance, and Root Mean Square Error between the predicted trajectory  $\hat{T}$  and the ground-truth trajectory  $T^*$ . The final term enforces endpoint accuracy by penalizing the distance between the predicted endpoint  $\hat{p}_N$  and the ground-truth endpoint  $p_M^*$ .

The model is guided by a carefully designed prompt that specifies both the reasoning and the answer requirements. The full prompt template is shown below:

```
{Question} First output the thinking process in <think> </think> tags and then
output the final answer in <answer> </answer> tags. Output the final answer in
the following JSON format: [[x1, y1], [x2, y2], ..., [xn, yn]]. Where each
coordinate pair represents a point in the image’s pixel space and the center of
the end effector needs to follow the coordinates to complete the task. Each hand
trajectory includes unknown number of [x, y] coordinate pairs. DO NOT OUTPUT ANY
ANSWER OR CONCLUSION IN THE THINK TAGS.
```

### D.6. Demand Prediction

The task is defined as demand prediction, where the model, given an image and a human demand instruction (e.g., “I am thirsty”), is required to output a two-dimensional coordinate corresponding to an object in the image that fulfills the demand (e.g., a water bottle or a juice box). A prediction is considered correct if the predicted point lies inside the ground-truth segmentation mask of the demanded object.

We construct the dataset for this task based on MO-DDN (Wang et al., 2024), which requires robots to ground a natural demand instruction to objects in the environment. MO-DDN itself is built upon the HSSD scene dataset (Khanna et al., 2024), together with a custom demand-object dataset. To build our data, we randomly sample a demand instruction and pair it with a scene containing a target object that satisfies the demand. We then crop and store the corresponding image, resulting in instruction-image pairs.

Following the original MO-DDN splits, we collect data separately from the training and testing tasks. Specifically, we use 3,000 instruction-image pairs as the training set and 1,000 pairs as the validation set, both sampled from the training tasks. For evaluation, we construct a test set of 5,000 instruction-image pairs sampled from the testing tasks.

We train the model for a single epoch on the training set and perform model selection based on validation accuracy. The checkpoint achieving the highest validation performance is then used for testing, and we report results on the test set.

We evaluate the model’s performance using a *Success Rate* metric, defined as the proportion of samples where the predicted coordinate falls within the ground-truth mask of the demanded object. Formally:

$$\text{Success Rate} = \frac{\sum_{i=1}^N \mathbb{I}(M_{\text{gt}}^{(i)}(C_{\text{pred}}^{(i)}) = 1)}{N}, \tag{28}$$

where  $N$  is the number of samples in the test set,  $C_{\text{pred}}^{(i)}$  denotes the predicted 2D coordinate  $(x, y)$  for the  $i$ -th sample, and  $M_{\text{gt}}^{(i)}$  is the ground-truth binary mask of the demanded object. The notation  $M_{\text{gt}}^{(i)}(C_{\text{pred}}^{(i)})$  indicates the mask value at the predicted location.  $\mathbb{I}(\cdot)$  is the indicator function that equals 1 if the condition holds and 0 otherwise.

The reward function for training consists of two complementary components: a *format reward* and an *accuracy reward*. The model must output predictions in the following structured format:

```
<think> xxx </think>
<answer> [d, d] </answer>
```

where the final answer corresponds to a 2D coordinate  $[d, d]$ , with  $d$  denoting an integer. The format reward is assigned 1 if the output strictly follows this structure, and 0 otherwise. The accuracy reward is assigned if and only if the predicted coordinate lies within the ground-truth object mask. These two rewards jointly ensure syntactically valid outputs and semantic correctness.

The model is guided by a prompt template that specifies both the thinking process and the final answer format. The full prompt is given below:

```
You are completing a navigation task where you need to detect objects from the image that fulfill a user’s demand. The user’s demand is {Question}. First output the thinking process in <think> </think> tags and then output the final answer in <answer> </answer> tags. Only output one point using [x, y] format that represents the target demanded object. DO NOT OUTPUT ANY ANSWER OR CONCLUSION IN THE THINK TAGS.
```

### D.7. OCR-based VQA

The task is defined as OCR-based Visual Question Answering (VQA), where the model, given an image containing textual information and a natural language question, is required to output a short natural language answer. The answer must be grounded in the image content and can involve both text extraction and reasoning over visual elements.

We construct the dataset by combining three OCR-based VQA benchmarks: *Document VQA* (Tito et al., 2021), *Infographics VQA* (Tito et al., 2021), and *Scene Text VQA* (Biten et al., 2019). Document VQA focuses on answering questions asked

over document images, which may contain printed, typewritten, and handwritten content (*e.g.*, letters, memos, reports). The answers are typically text spans taken verbatim from the document. Infographics VQA considers questions over infographic images containing charts, diagrams, or other structured visual data, where answers are not always explicitly extracted text but can include inferred information. Scene Text VQA consists of natural scene images with embedded text (*e.g.*, storefronts, street signs). The model must jointly leverage OCR reading and visual understanding to answer the questions.

From each of the three training sets, we randomly select 3,000 samples, resulting in a combined training set of 9,000 samples. Additionally, we construct a validation set of 1,500 samples (also drawn from the training splits), while the official validation sets of each benchmark are used as our test set.

The model is trained for a single epoch on the 9,000-sample mixed training set. Model selection is performed based on validation performance, and the checkpoint achieving the highest validation score is reported on the test sets.

The evaluation metric is the *Average Normalized Levenshtein Similarity* (ANLS), which measures the string-level similarity between the predicted and ground-truth answers. ANLS accounts for OCR errors by softly penalizing recognition mistakes. A threshold  $\tau = 0.5$  is applied to determine whether a predicted answer is considered valid. Formally, ANLS is defined as:

$$\text{ANLS} = \frac{1}{N} \sum_{i=0}^N \left( \max_j s(a_{ij}, o_{q_i}) \right), \tag{29}$$

$$s(a_{ij}, o_{q_i}) = \begin{cases} 1 - NL(a_{ij}, o_{q_i}), & \text{if } NL(a_{ij}, o_{q_i}) < \tau, \\ 0, & \text{if } NL(a_{ij}, o_{q_i}) \geq \tau, \end{cases} \tag{30}$$

where  $N$  is the number of questions,  $M$  is the number of ground-truth answers per question,  $a_{ij}$  is the  $j$ -th ground-truth answer for the  $i$ -th question  $q_i$ , and  $o_{q_i}$  is the predicted answer.  $NL(\cdot)$  denotes the normalized Levenshtein distance.

The reward function consists of a *format reward* and an *accuracy reward*. The model must output answers in the following structured format:

```
<think> xxx </think>
<answer> xxx </answer>
```

The format reward is 1 if the output strictly follows this structure, and 0 otherwise. The accuracy reward corresponds to the ANLS score of the predicted answer for the current question.

The model is guided by the following prompt template:

```
{Question} First output the thinking process in <think> </think> tags and then
output the final answer in <answer> </answer> tags. The answer should be a
natural language text. The answer should be found in the image. DO NOT OUTPUT
ANY ANSWER OR CONCLUSION IN THE THINK TAGS.
```

### D.8. Simulator-based Visual Manipulation

The task is defined as a simulator-based visual manipulation problem where, given a single RGB observation of a manipulation scene, the model must specify a contact point  $(x, y)$  on the object at which a sucker should attempt to manipulate. The model’s output must be grounded in the visual observation and may require reasoning about object geometry, affordances, and reachable contact locations.

We construct the dataset and evaluation splits based on the PartNet Mobility dataset (Xiang et al., 2020) and the ManipLLM experimental setup (A **crucial point is that we have followed their setting by using suckers as the end effectors for the robotic arms.**). For training, we adopt the same 20 training categories as ManipLLM, consisting of 1,043 object instances. Training scenes are generated following the SAPIEN simulator (Xiang et al., 2020) setup and ManipLLM scene configurations. For testing, we use the open-sourced ManipLLM test set, which contains approximately 1,830 successful test samples spanning both Seen and Unseen objects. To better evaluate model generalization to novel viewpoints, we further construct a camera-perturbed test set by modifying each test sample: the camera orientation vector  $[0, 0, 0]$  is replaced by  $[x, y, z]$  where each of  $x, y, z$  is sampled uniformly from the signed interval  $\pm[0.2, 0.6]$ . This perturbation preserves other

scene properties while intentionally stressing viewpoint robustness. In order to simplify control and isolate contact selection, the sucker approach direction in all experiments is fixed to be the surface normal at the chosen manipulation point  $(x, y)$ .

The required output must follow a strict format consisting of a reasoning trace and a final contact point, written as:

```
<think> xxxx </think>
<answer> (d,d) </answer>
```

The evaluation metric is Success Rate, following ManipLLM’s criterion based on the manipulated object’s displacement after the scripted sucker motion. Formally, given  $N$  trials,

$$\text{SuccessRate} = \frac{1}{N} \sum_{i=1}^N \mathbb{I}\{\text{trial}_i \text{ is successful according to ManipLLM’s displacement criterion}\},$$

where  $\mathbb{I}\{\cdot\}$  is the indicator function. We report Success Rate on the camera-perturbed test sets, and further provide breakdowns by Seen vs. Unseen objects.

The reward function during GRPO training consists of a format reward and a task reward. The format reward is 1 if the output strictly follows the required structure and 0 otherwise. The task reward is 1 if the manipulation attempt succeeds according to ManipLLM’s displacement criterion and 0 otherwise. The overall reward is defined as

$$R_{\text{total}} = R_{\text{format}} + R_{\text{task}},$$

so that only properly formatted and successful outputs receive credit. This ensures that malformed answers cannot be rewarded even if the manipulation itself succeeds.

All experiments are conducted with Qwen2.5-VL-3B as the base model. We train using GRPO for 4,000 optimization steps, selecting checkpoints based on validation success rate. The validation set is constructed by sampling held-out scenes from the same 20 training categories without overlap with the test split. The prompt used in training is as follows:

```
"system": "You are an intelligent manipulator. A conversation between
User and Assistant. The user asks a question, and the Assistant solves
it. The assistant first thinks about the reasoning process in the mind
and then provides the user with the answer. The reasoning process and
answer are enclosed within <think> </think> and <answer> </answer> tags,
respectively, i.e. <think> reasoning process here </think><answer> answer
here </answer>."
```

```
"user": "Specify the contact point (x, y) of manipulating the object.
The camera resolution is:'width': 336, 'height': 336, Output format:
<think>your thinking process</think> <answer>(x,y)</answer>"
```

## E. Details in Training

### E.1. Training Hyperparameters

We summarize the key hyperparameters used in our GRPO training experiments in Tab. 9. The settings are organized into general, training, and LoRA-related categories for clarity.

### E.2. SFT Details

For all Supervised Fine-Tuning (SFT) baselines, we train for 5 epochs. All other settings are kept consistent with GRPO, including the dataset, model selection criteria, and metric calculation.

### E.3. Generation Configure

Our model is trained using the Hugging Face transformers library (version 4.51.3). During inference, we customize the decoding strategy via the GenerationConfig class. Specifically, we set temperature=1.0 and do\_sample=True

Table 9. Hyperparameters for GRPO training.

Hyperparameter Group	Parameter	Value
<i>Training Configuration</i>		
	Model	Qwen2.5-VL-3B-Instruct
	Optimizer	AdamW
	Learning Rate ( $\eta$ )	$1 \times 10^{-5}$
	Batch Size	1
	Gradient Accumulation Steps	1
	Total Training Epochs	1
	Max Completion Length	4096
	Data Seed	42
	Floating Point Precision	bfloat16
	Gradient Checkpointing	true
	Flash Attention 2	true
<i>PEFT (LoRA) Configuration</i>		
	LoRA Rank ( $r$ )	64
	LoRA Alpha ( $\alpha$ )	128
	LoRA Dropout	0.05
<i>GRPO-specific Configuration</i>		
	Beta ( $\beta$ )	0.04
	Epsilon High ( $\epsilon_H$ )	0.28
	Epsilon Low ( $\epsilon_L$ )	0.2
<i>Model Specific Configuration</i>		
	Freeze Vision Modules	true

to enable stochastic sampling. We also define `stop_strings=["</think>", "</analysis>"]` only when generating thoughts. The remaining parameters are maintained at their default settings.

## F. Case Study and Visualization

To provide a more intuitive and in-depth analysis of our model’s performance, this section presents a series of curated case studies and visualizations. These examples encompass a range of key tasks, including object detection ( Fig. 3 and Fig. 4) and trajectory prediction (Fig. 5 and Fig. 6). Our aim is to leverage these concrete scenarios to delve into the model’s behavior, decision-making logic, and inherent strengths and limitations.

Specifically, in the simulator-based visual manipulation task, we visualize the distribution of the target operation points over multiple sampling attempts in Fig. 7. Green points indicate successful manipulations, while red points represent failures. This visualization demonstrates the robustness of our model.

## G. More Experimental Analysis

In this section, we further present some experimental results, including inconsistency analysis, the accuracy reward curves during training, and an analysis of the richness of reward signal.

### G.1. Inconsistency Analysis

We quantify the inconsistency between thoughts and answers during training. For a thought  $th_i$  with  $M$  answers, if  $\text{sign}(A(th_i)) \neq \text{sign}(A(ans_{i,j}))$ , we mark it as inconsistent. The inconsistency rate is defined as  $\text{InconsistencyRate} = \frac{1}{KM} \sum_{i=1}^K \sum_{j=1}^M \mathbb{I}[A(th_i)A(ans_{i,j}) < 0]$ , where  $\mathbb{I}[\cdot]$  denotes the indicator function, which equals 1 if the condition inside holds and 0 otherwise.

Under the T4A4 setting, the inconsistency rate is **25.65%** for trajectory prediction and **24.83%** for object detection. Notably, this ratio is also indicative for GRPO baselines (T4A1, T8A1, T16A1), even though they do not explicitly generate multiple answers per thought and thus cannot directly compute it, since they share the same generation hyperparameters (*e.g.*, temperature, top- $k$ , and top- $p$  sampling). This observation further supports our claim that inconsistency is common in GRPO’s training. Moreover, this inconsistency implicitly undermines model training.

### G.2. Accuracy Reward Curve

We present the accuracy reward curves for five visual tasks in Object Detection (Fig. 8), Affordance Prediction (Fig. 9), Demand Prediction (Fig. 10), OCR-based VQA (Fig. 11) and Trajectory Prediction (Fig. 12). During the curve plotting process, we smooth the curve using a moving average method with a window size of 200. The curves demonstrate that T4A4 (red) exhibits performance comparable to that of T16A1 (blue) in the majority of cases, at times showing a marginal advantage.

### G.3. Richness of Reward Signals

For tasks with binary (0–1) rewards, such as Code, Math, Affordance Prediction, Demand Prediction, and Simulator-based Visual Manipulation, we measure the proportion of samples whose total reward is positive, which we refer to as the *NoZeroRate*. Formally, it is defined as

$$\text{NoZeroRate} = \frac{1}{T} \sum_{t=1}^T \mathbf{1} \left\{ \left( \sum_{i=1}^K \sum_{j=1}^M \text{AccR}_{i,j}^t \right) > 0 \right\}, \tag{31}$$

where  $\mathbf{1}\{\cdot\}$  denotes the indicator function, which equals 1 if the condition holds and 0 otherwise. Here,  $T$  is the total number of time steps,  $t$  indexes a specific time step,  $K$  is the number of thoughts,  $M$  is the number of answers per thought, and  $\text{AccR}_{i,j}^t$  denotes the accuracy reward associated with the  $j$ -th answer under the  $i$ -th thought at time step  $t$ . Intuitively, a higher *NoZeroRate* indicates a lower proportion of advantage collapse (*i.e.*, all advantage values being zero), and thus a larger fraction of samples contributing effective gradient information.

The statistical results are reported in Tab. 10. We observe that T4A4 achieves the second-highest *NoZeroRate* across all

Table 10. NoZeroRate on Different Task. TN: The number of thoughts; AN: The number of answers per thought. **Bold** indicates the best performance and *italics* indicate the second-best performance.

	TN	AN	Code	Math	Affordance	Demand	Sim Manip
GRPO	4	1	26.71%	19.14%	85.10%	46.37%	38.20%
GRPO	8	1	36.57%	27.71%	94.37%	62.07%	/
GRPO	16	1	<b>43.71%</b>	<b>43.29%</b>	<b>97.17%</b>	<b>70.20%</b>	/
GRPO-MA	4	4	41.86%	34.71%	96.70%	66.47%	<b>85.05%</b>

tasks, only behind T16A1. This result suggests that T4A4 strikes a favorable balance between the number of thoughts and the number of answers per thought, leading to a high probability that at least one sampled answer yields a non-zero reward. In particular, compared with T4A1, T4A4 exhibits a substantially higher NoZeroRate, indicating that generating multiple answers per thought significantly reduces the likelihood of advantage collapse.

This comparison also addresses a potential concern regarding whether sampling multiple answers conditioned on the same thought truly produces diverse solutions, rather than near-duplicate ones. If answers sampled from a single thought were largely identical, then increasing the number of answers per thought would be unlikely to introduce higher NoZeroRate, and configurations such as T4A4 and T4A1 would be expected to exhibit similar NoZeroRates. However, under our high-temperature sampling regime, we observe a clear gap between the NoZeroRates of T4A4 and T4A1. This gap indicates that additional answers sampled from the same thought substantially increase the probability of observing at least one non-zero reward, thereby leading to a higher NoZeroRate. This provides indirect but quantitative evidence that multi-sampling under a fixed thought yields diverse and effective answers within our framework.

#### G.4. Wall-clock Time

We provide wall-clock time to further demonstrate the improvement in training efficiency achieved by the GRPO-MA algorithm. We pick two multimodal tasks and one text reasoning task as examples. The results are shown in Fig. 13, Fig. 14, and Fig. 15. As shown in the figure, GRPO-MA achieves the peak performance of various baselines in a shorter time.

#### G.5. Grad-norm and GSS Curve

We provide complete Grad Norm and GSS curves, shown in Fig. 16, Fig. 17 and Fig 18. Smaller fluctuations in the Grad Norm curve and lower GSS values indicate fewer gradient spikes during training, resulting in more stable training. The grad norm curve and GSS curve corresponding to GRPO-MA both exhibit smaller fluctuations and GSS values.

#### G.6. More Results on Code and Math

To further examine the generality of our variance-reduction mechanism, we additionally evaluate GRPO-MA on two widely used mathematical and coding benchmarks: GSM8K (Cobbe et al., 2021) for math reasoning and HumanEval (Chen et al., 2021a) for code generation. These experiments use the same training configuration as our main results, with models trained on the DAPO dataset. For GSM8K, we report the Pass@1 accuracy obtained by running the checkpoint trained for mathematical reasoning. For HumanEval, we report Pass@1 and Pass@5 to assess both direct correctness and sampling-based performance. These findings reinforce our claim that answer-level multi-sampling provides a simple, general, and effective variance-reduction strategy that benefits both mathematical reasoning and code generation tasks. The consolidated results are presented in Table 11.

#### H. Usage of LLMs

We employ a Large Language Model (LLM) to refine the manuscript, with a focus on correcting grammatical errors and enhancing overall readability.

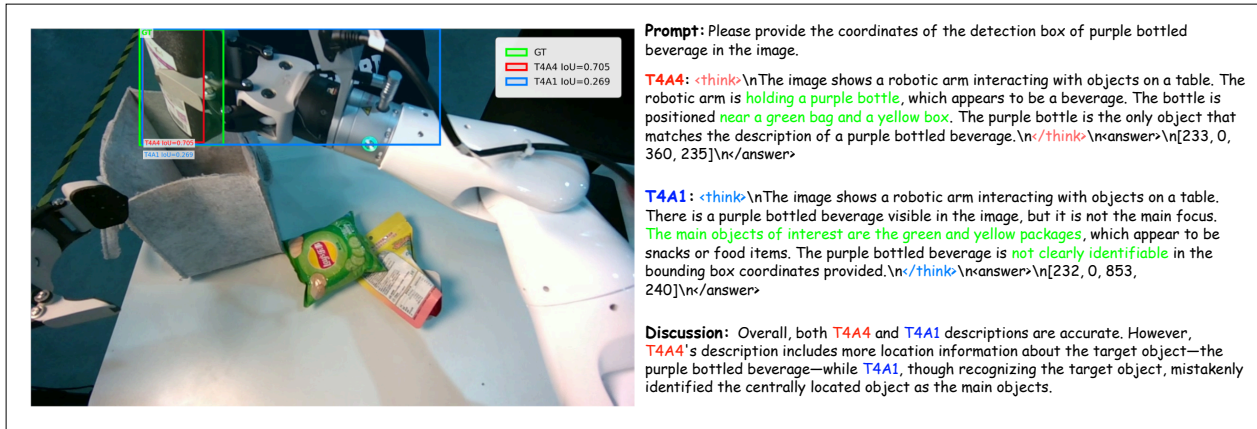


Figure 3. A case study comparing the baseline GRPO with our proposed GRPO-MA on a referring expression grounding task. The prompt is to locate the “purple bottled beverage”. The baseline model, GRPO (T4A1), recognizes the target’s existence but its reasoning is distracted by other salient objects (the snacks), leading to a failure in grounding. In contrast, our GRPO-MA (T4A4) correctly reasons about the scene’s context, focuses on the target object held by the robotic arm, and successfully provides the precise bounding box. This demonstrates the superior robustness of GRPO-MA in complex scene understanding and reasoning.

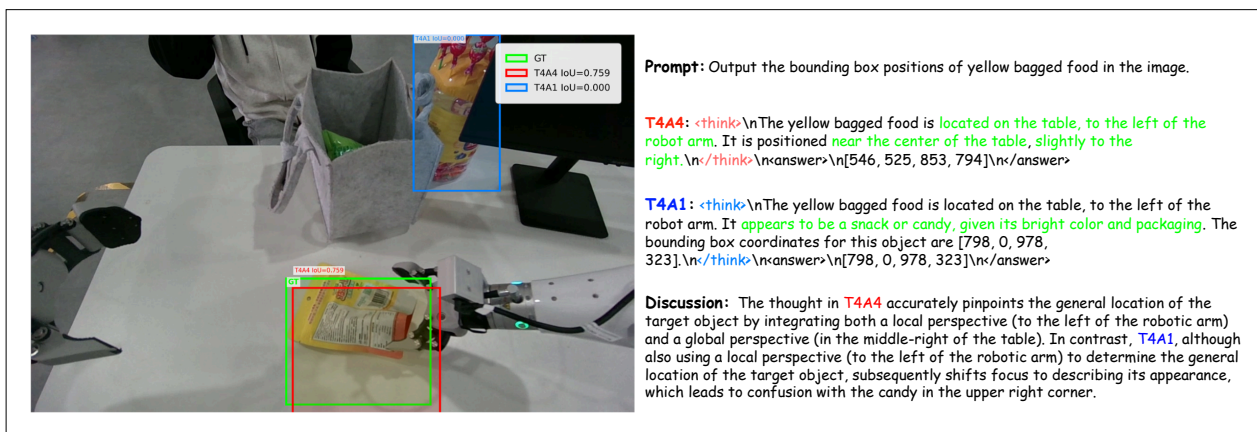


Figure 4. Case Study on Object Detection Green text indicates key reasoning content.

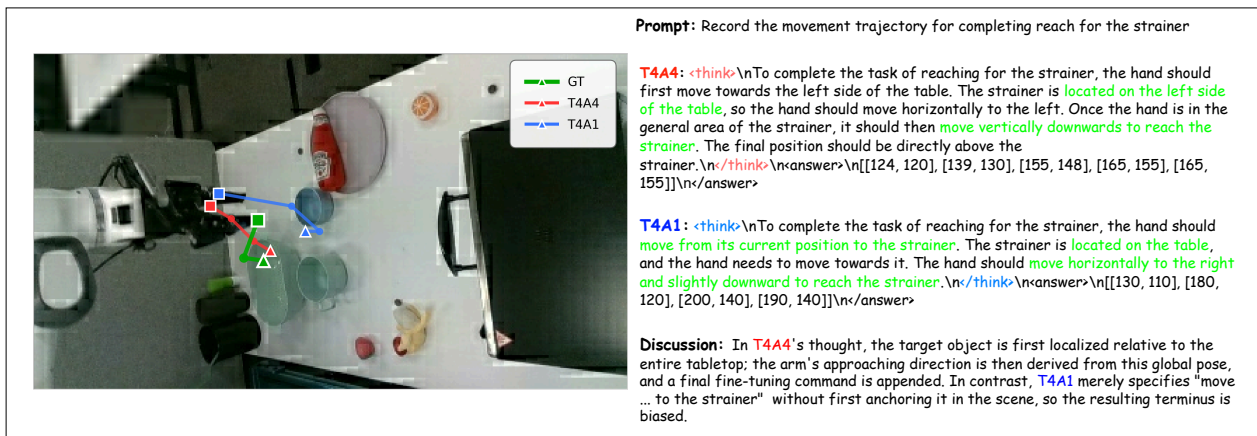


Figure 5. Case Study on Trajectory Prediction Green text indicates key reasoning content.

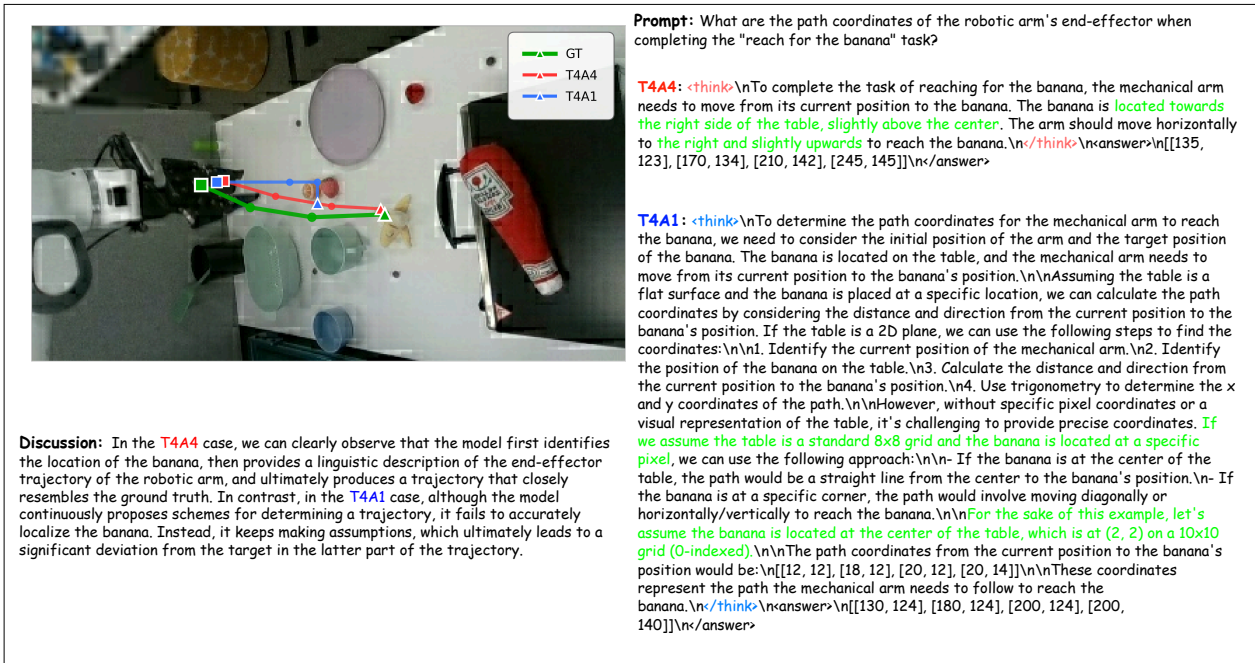


Figure 6. Case Study on Trajectory Prediction Green text indicates key reasoning content.

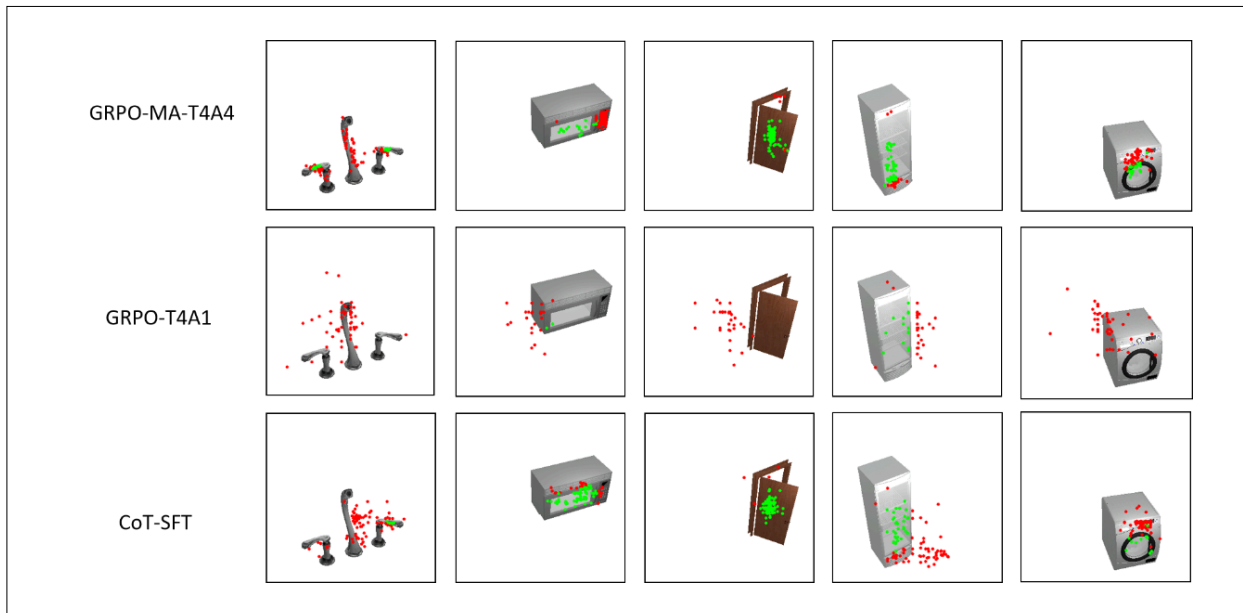


Figure 7. Visualization on Simulator-based Visual Manipulation Red dots indicate failures, while green dots represent successes. We can observe that most GRPO-MA-T4A4 points are located on the object. In contrast, GRPO-T4A1 frequently misses the object, resulting in a lower success rate.

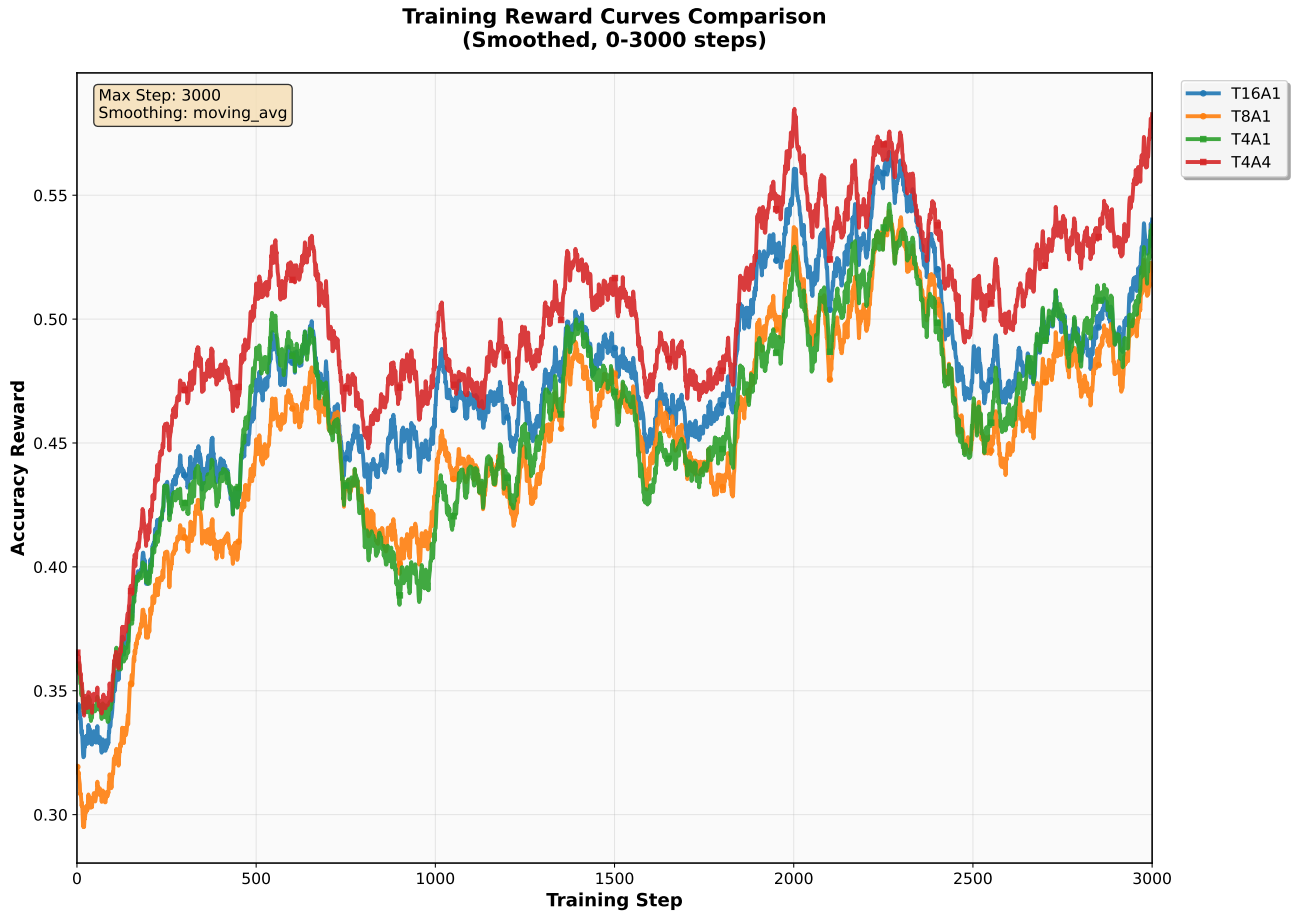


Figure 8. Accuracy Reward Curve on Object Detection

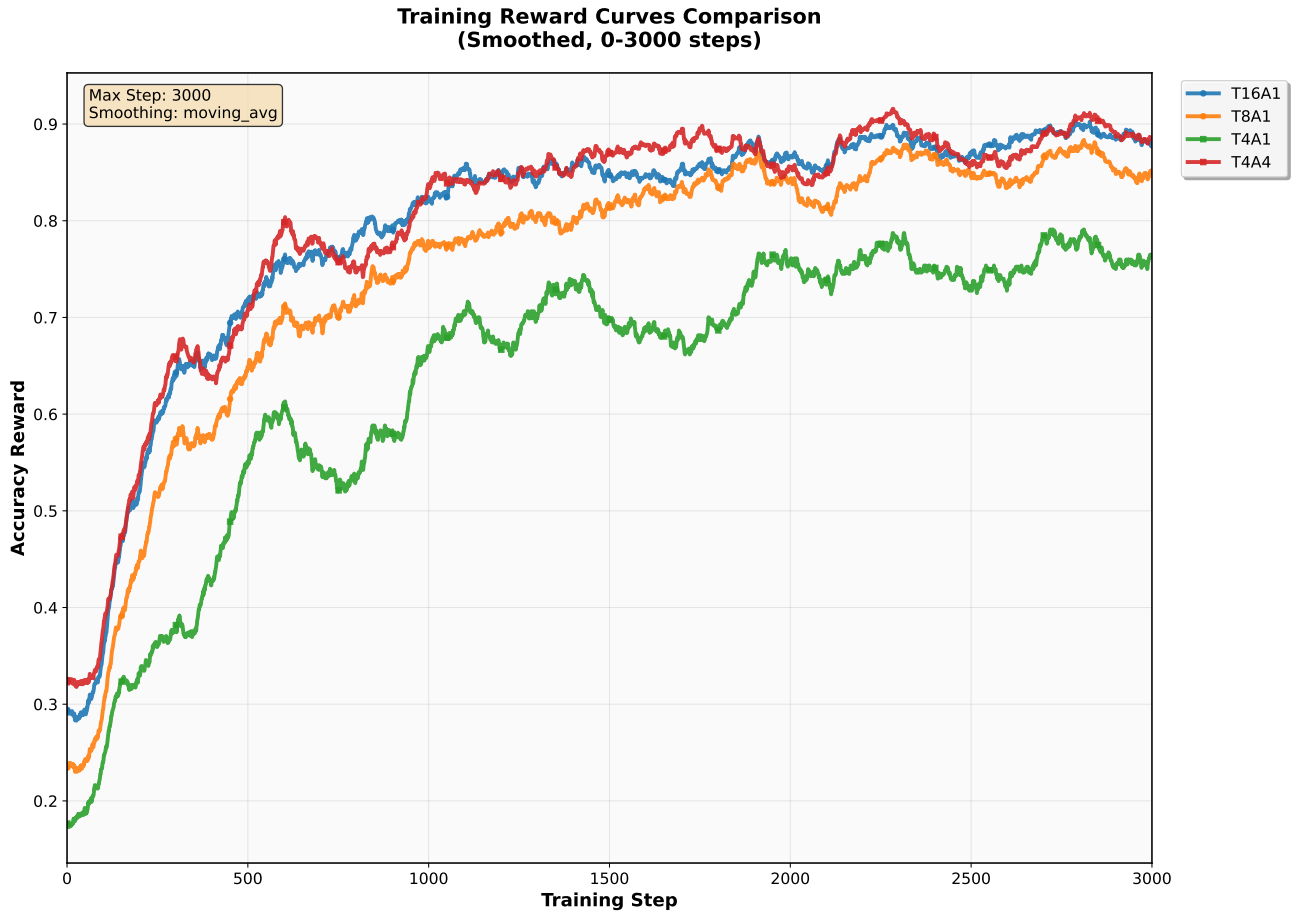


Figure 9. Accuracy Reward Curve on Affordance Prediction

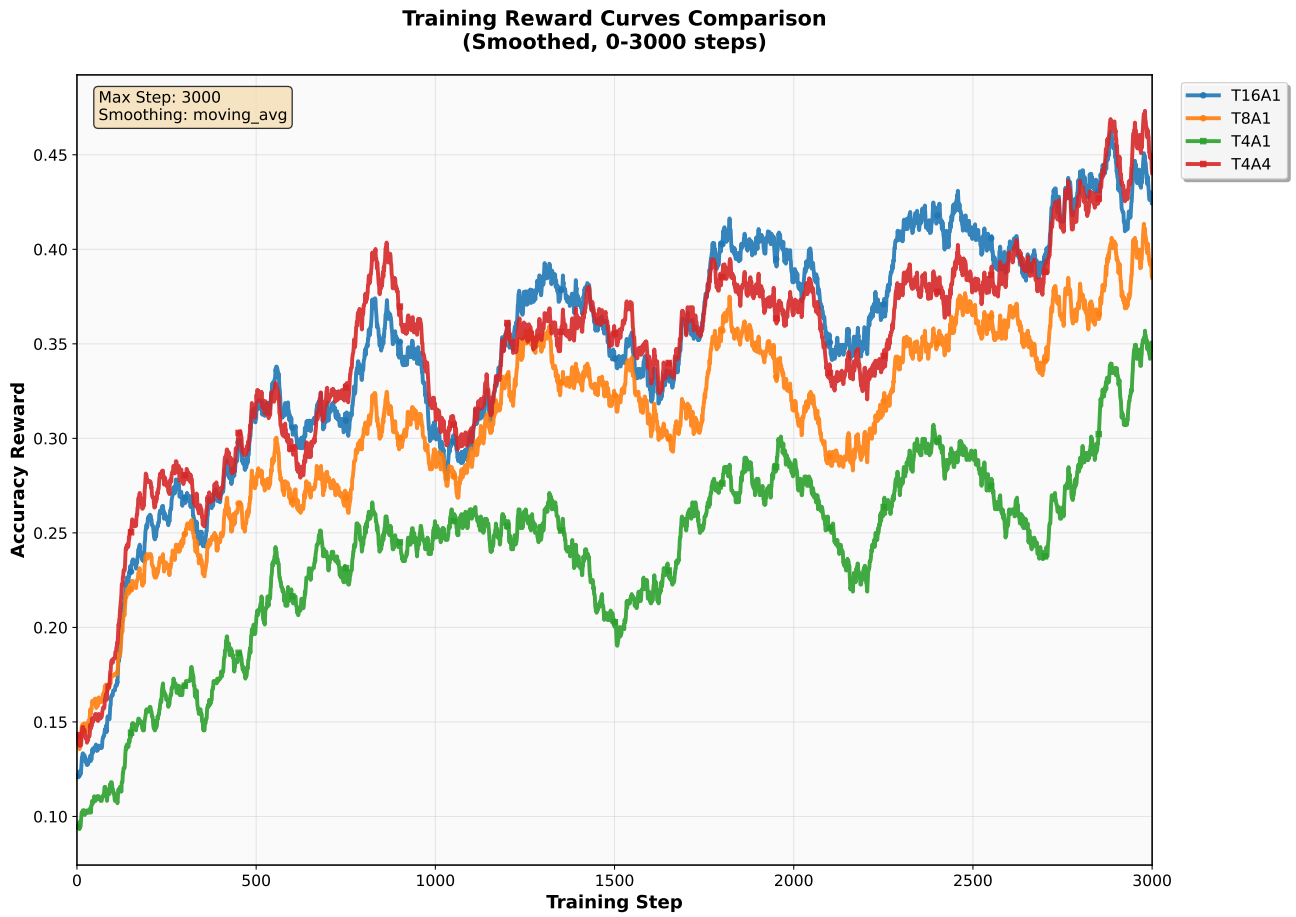


Figure 10. Accuracy Reward Curve on Demand Prediction

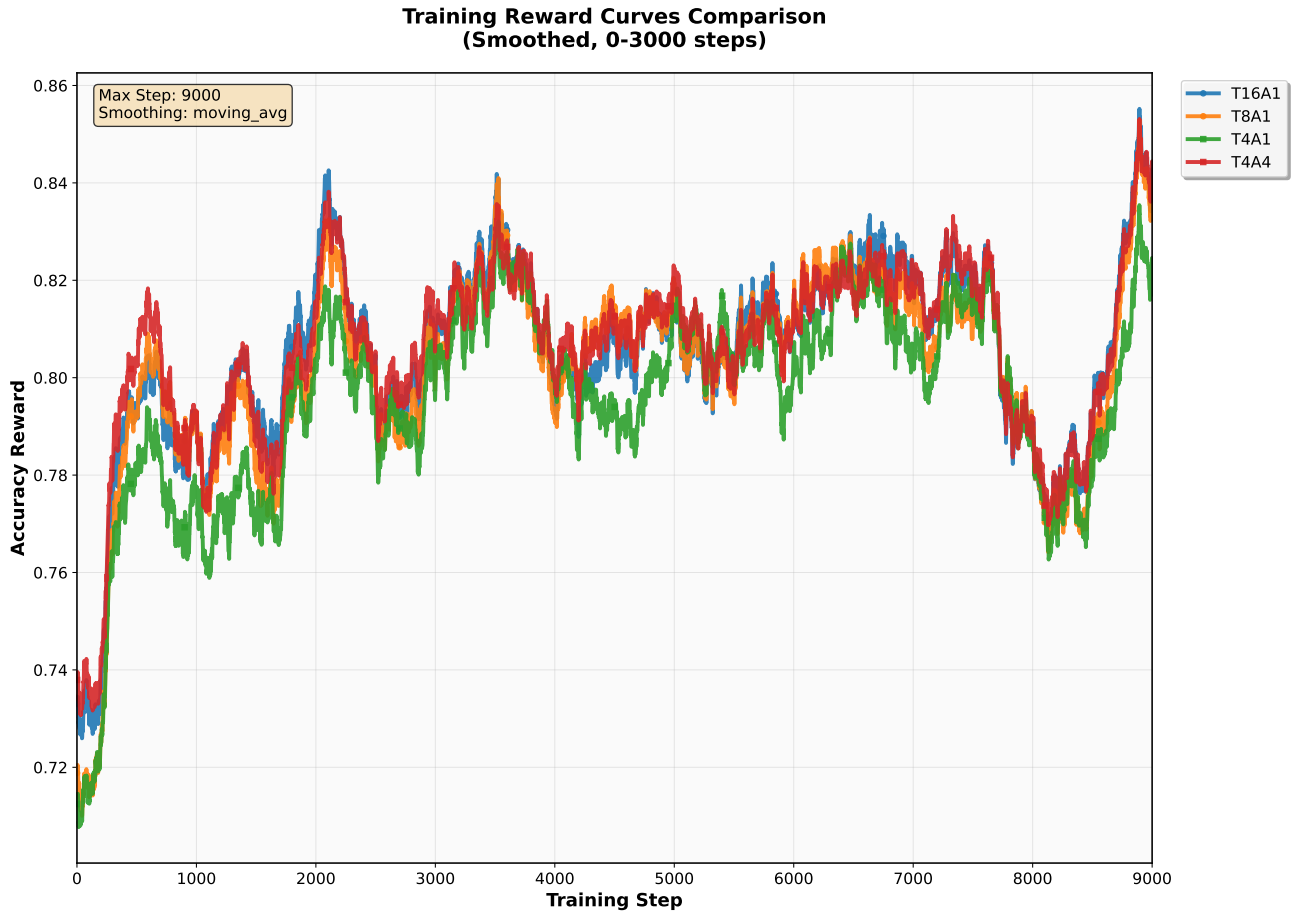


Figure 11. Accuracy Reward Curve on OCR-based VQA

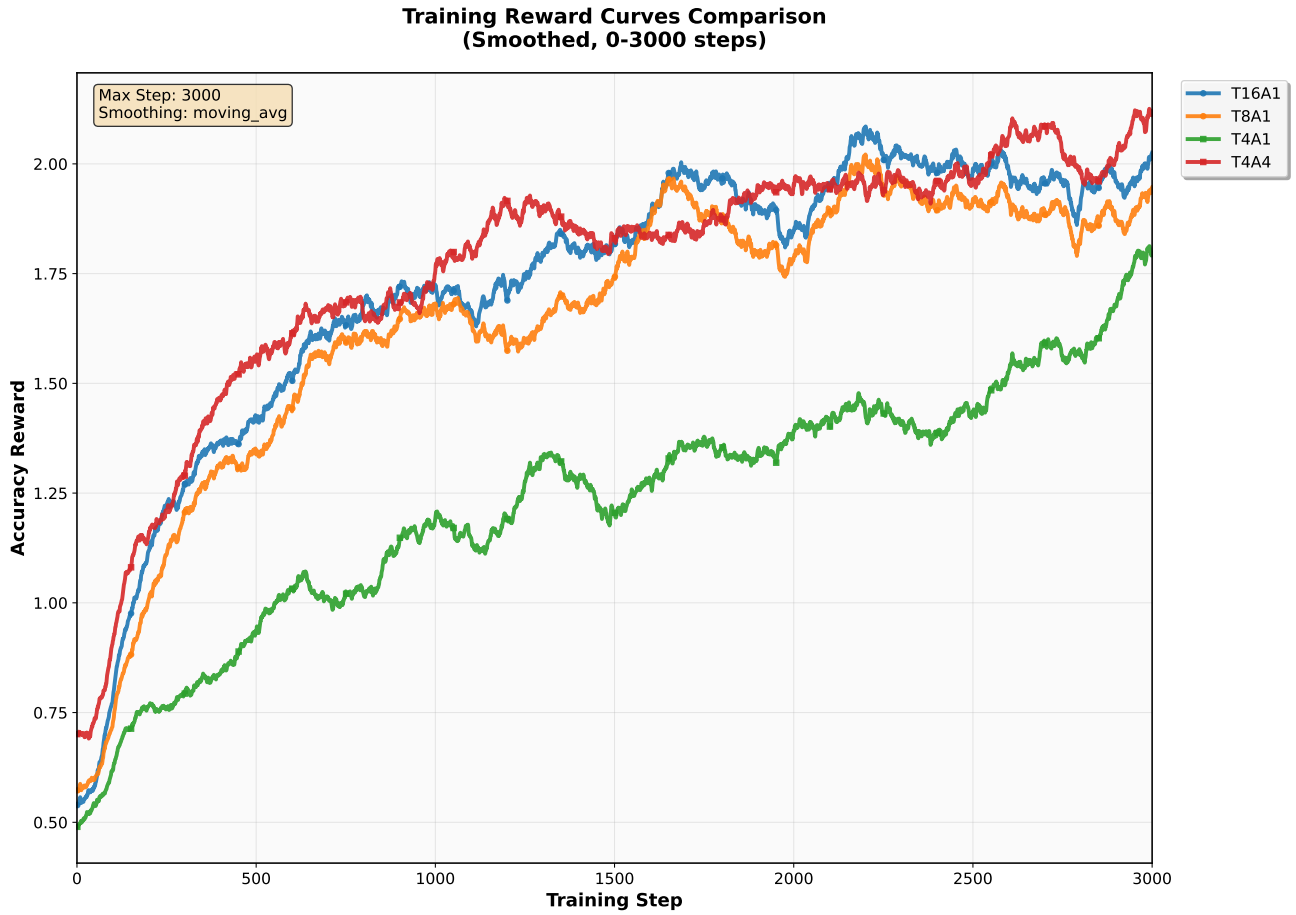


Figure 12. Accuracy Reward Curve on Trajectory Prediction

## Why Tree-Style Branching Matters

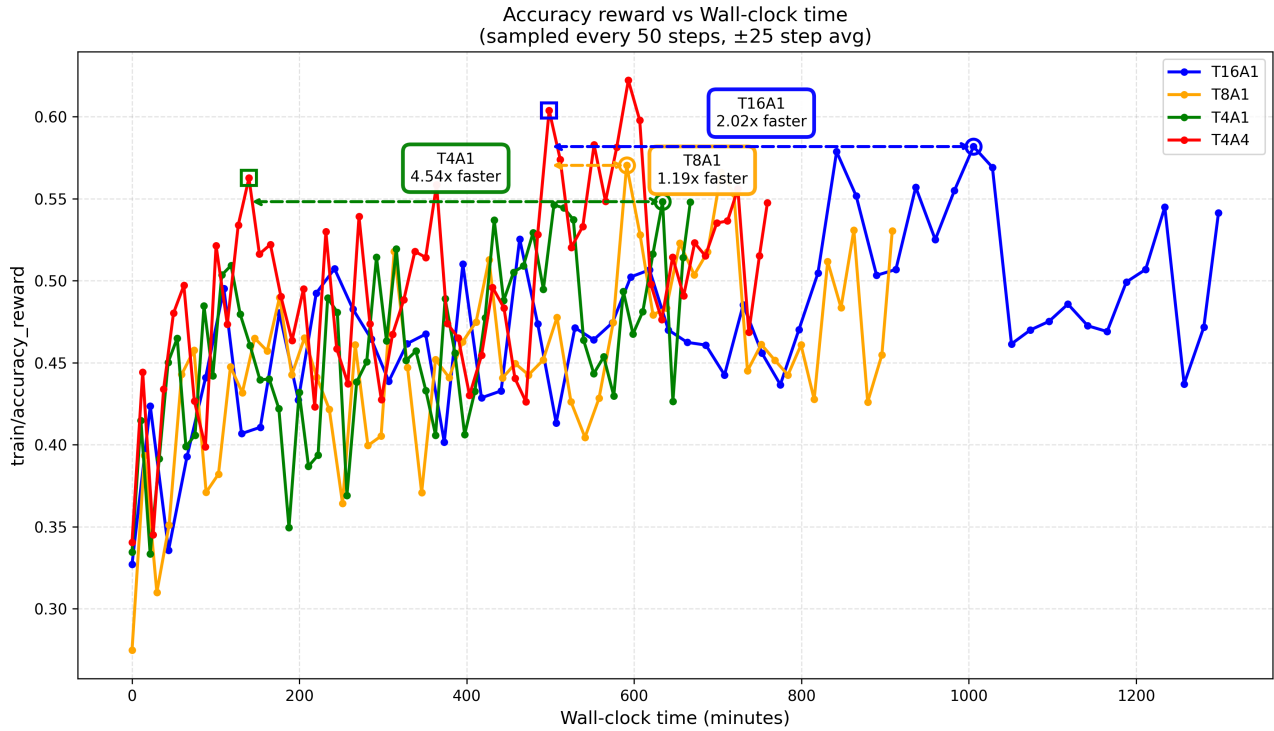


Figure 13. Wall-clock Time on Object Detection

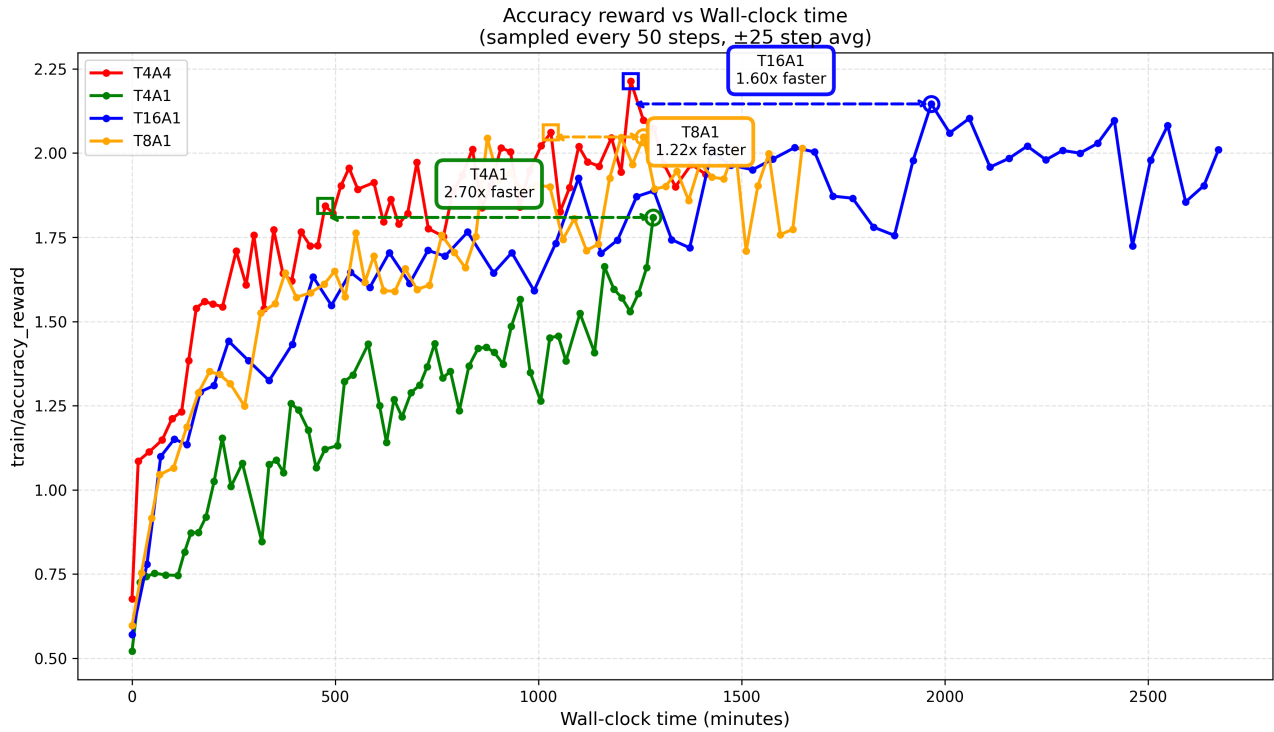


Figure 14. Wall-clock Time on Trajectory Prediction

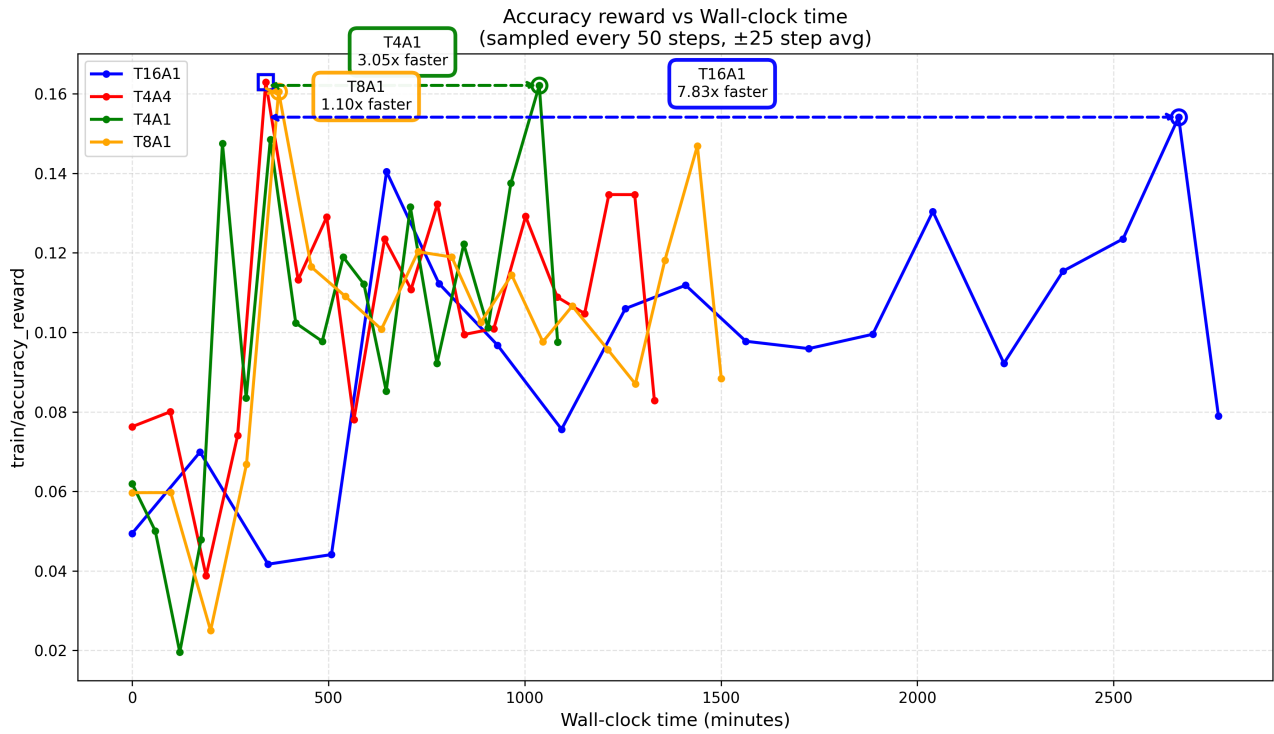


Figure 15. Wall-clock Time on Code

Object Detection | grad\_norm & GSS

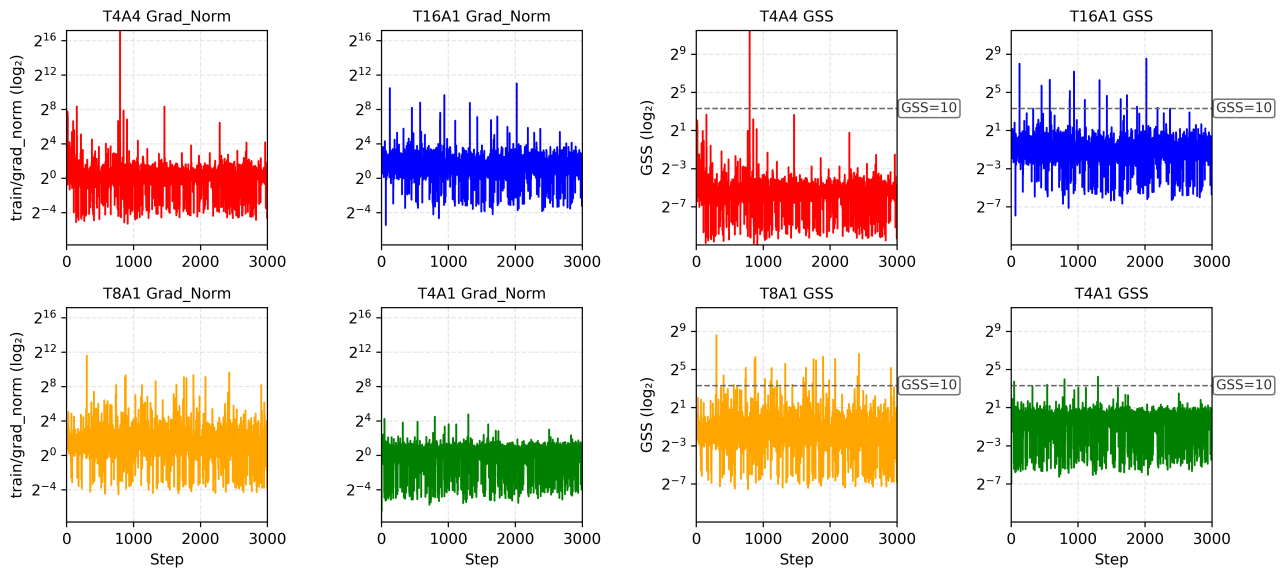


Figure 16. Grad Norm and GSS on Object Detection

Trajectory Prediction | grad\_norm & GSS

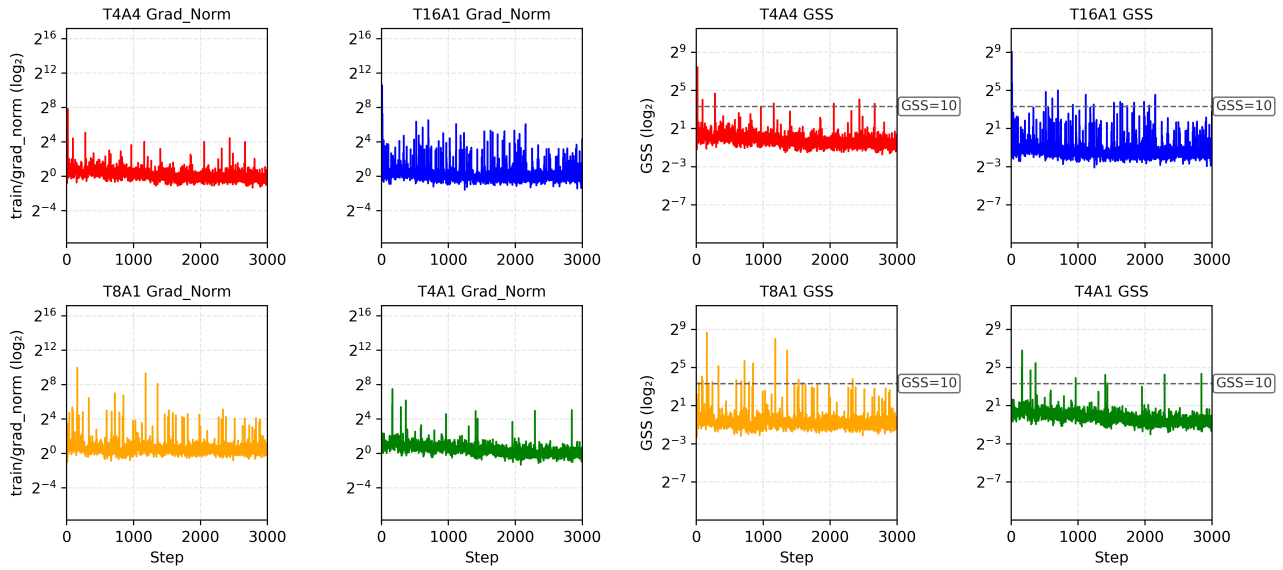


Figure 17. Grad Norm and GSS on Trajectory Prediction

Code | grad\_norm & GSS

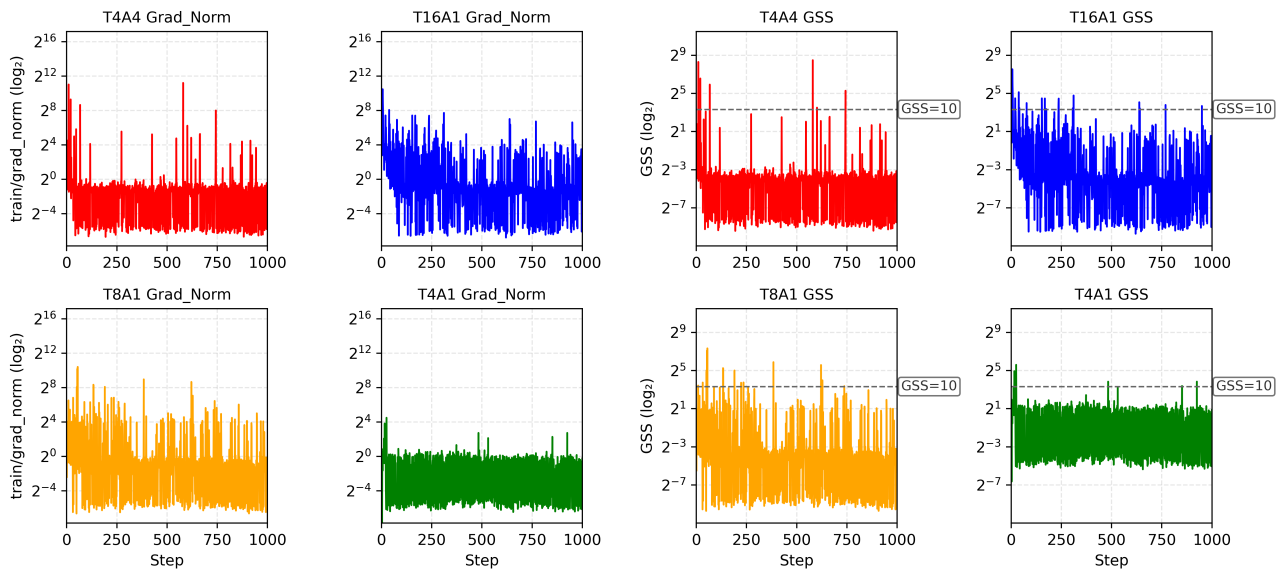


Figure 18. Grad Norm and GSS on Code

Table 11. Additional Results on GSM8K (Math) and HumanEval (Code). TN: Number of thoughts; AN: Number of answers per thought. Bold indicates the best performance among GRPO variants.

Model	TN	AN	GSM8K (Math)	HumanEval (Code)	
			Pass@1	Pass@1	Pass@5
GRPO	4	1	62.54	56.10	82.93
GRPO	8	1	64.67	56.83	82.93
GRPO	16	1	65.13	57.80	85.37
GRPO-MA	4	4	<b>70.58</b>	<b>58.66</b>	<b>87.20</b>